

ORIGINAL PAPER

Open Access



Origins of hydrocarbons in the Geneva Basin: insights from oil, gas and source rock organic geochemistry

Damien Do Couto^{1*} , Sylvain Garel^{2,3}, Andrea Moscariello⁴, Samer Bou Daher^{5,7}, Ralf Littke⁵ and Philipp Weniger⁶

Abstract

An extensive subsurface investigation evaluating the geothermal energy resources and underground thermal energy storage potential is being carried out in the southwestern part of the Swiss Molasse Basin around the Geneva Canton. Among this process, the evaluation of the petroleum source-rock type and potential is an important step to understand the petroleum system responsible of some oil and gas shows at surface and subsurface. This study provides a first appraisal of the risk to encounter possible undesired occurrence of hydrocarbons in the subsurface of the Geneva Basin. Upon the numerous source-rocks mentioned in the petroleum systems of the North Alpine Foreland Basin, the marine Type II Toarcian shales (Lias) and the terrigenous Type III Carboniferous coals and shales have been sampled from wells and characterized with Rock-Eval pyrolysis and GC-MS analysis. The Toarcian shales (known as the Posidonia shales) are showing a dominant Type II organic matter composition with a Type III component in the Jura region and the south of the basin. Its thermal maturity (~0.7 VRr%) shows that this source-rock currently generates hydrocarbons at depth. The Carboniferous coals and shales show a dominant Type III organic matter with slight marine to lacustrine component, in the wet gas window below the Geneva Basin. Two bitumen samples retrieved at surface (Roulave stream) and in a shallow borehole (Satigny) are heavily biodegraded. Relative abundance of regular steranes of the Roulave bitumen indicates an origin from a marine Type II organic matter. The source of the Satigny bitumen is supposedly the same even though a deeper source-rock, such as the lacustrine Permian shales expelling oil in the Jura region, can't be discarded. The oil-prone Toarcian shales in the oil window are the most likely source of this bitumen. A gas pocket encountered in the shallow well of Satigny (Geneva Canton), was investigated for molecular and stable isotopic gas composition. The analyses indicated that the gas is made of a mixture of microbial (very low $\delta^{13}C_1$) and thermogenic gas. The isotopic composition of ethane and propane suggests a thermogenic origin from an overmature Type II source-rock (> 1.6 VRr%) or from a terrigenous Type III source at a maturity of ~1.2 VRr%. The Carboniferous seems to be the only source-rock satisfying these constraints at depth. The petroleum potential of the marine Toarcian shales below the Geneva Basin remains nevertheless limited given the limited thickness of the source-rock across the area and does not pose a high risk for geothermal exploration. A higher risk is assigned to Permian and Carboniferous source-rocks at depth where they reached gas window maturity and generated large amount of gas below sealing Triassic evaporites. The large amount of faults and fractures cross-cutting the entire

Editorial handling: Wilfried Winkler.

*Correspondence: damien.do_couto@sorbonne-universite.fr

¹ Sorbonne Université, CNRS-INSU, Institut Des Sciences de La Terre Paris, ISTE P UMR 7193, 75005 Paris, France

Full list of author information is available at the end of the article



© The Author(s) 2021. This article is licensed under a Creative Commons Attribution 4.0 International License, which permits use, sharing, adaptation, distribution and reproduction in any medium or format, as long as you give appropriate credit to the original author(s) and the source, provide a link to the Creative Commons licence, and indicate if changes were made. The images or other third party material in this article are included in the article's Creative Commons licence, unless indicated otherwise in a credit line to the material. If material is not included in the article's Creative Commons licence and your intended use is not permitted by statutory regulation or exceeds the permitted use, you will need to obtain permission directly from the copyright holder. To view a copy of this licence, visit <http://creativecommons.org/licenses/by/4.0/>.

stratigraphic succession in the basin certainly serve as preferential migration pathways for gas, explaining its presence in shallow stratigraphic levels such as at Satigny.

Keywords: Geneva Basin, Hydrocarbons, Organic geochemistry, Toarcian, Permo–Carboniferous

1 Introduction

In the past few years, several projects aiming at assessing the potential for deep renewable geo-energy and the CO₂ Capture and Storage (CCS) feasibility have originated in Europe and more specifically in Switzerland where the future provision of energy is challenging both the industry and the scientific community (Chevalier et al. 2010; Leu and Siddiqi 2013; Moscariello 2019; Moscariello et al. 2020a). In this context, the interpretation of the subsurface geology and the reliable assessment of all potential energy resources (both fossil and renewable) are essentials to avoid any conflict of subsurface use and to quantify the risk of encountering undesired hydrocarbons accumulations while exploring for geothermal resources. Indeed, recent thermal modelling in the St. Gallen area revealed that a petroleum system involving deep gas-prone Permo–Carboniferous grabens, favored accumulation of gas in the lowermost Mesozoic units where a 3.5 magnitude earthquake was triggered containing a gas kick (Omodeo-Salé et al. 2020).

In the past century, conventional petroleum exploration took place in Europe in the search for oil and gas, and in particular in the North Alpine Foreland Basin extending from France to Austria. This exploration phase resulted in the acquisition of hundreds of 2D seismic lines both in France and Switzerland (Capar et al. 2015; Sommaruga et al. 2012) as well as 37 deep wells drilled in Switzerland (Lahusen 1992; Leu 2012) and 15 deep wells drilled in France around the Geneva Basin area (Moscariello 2019). Despite the detection of numerous oil and gas shows at the surface and in the subsurface, no major conventional petroleum accumulation has been found so far in the Swiss Molasse Basin (Leu 2012).

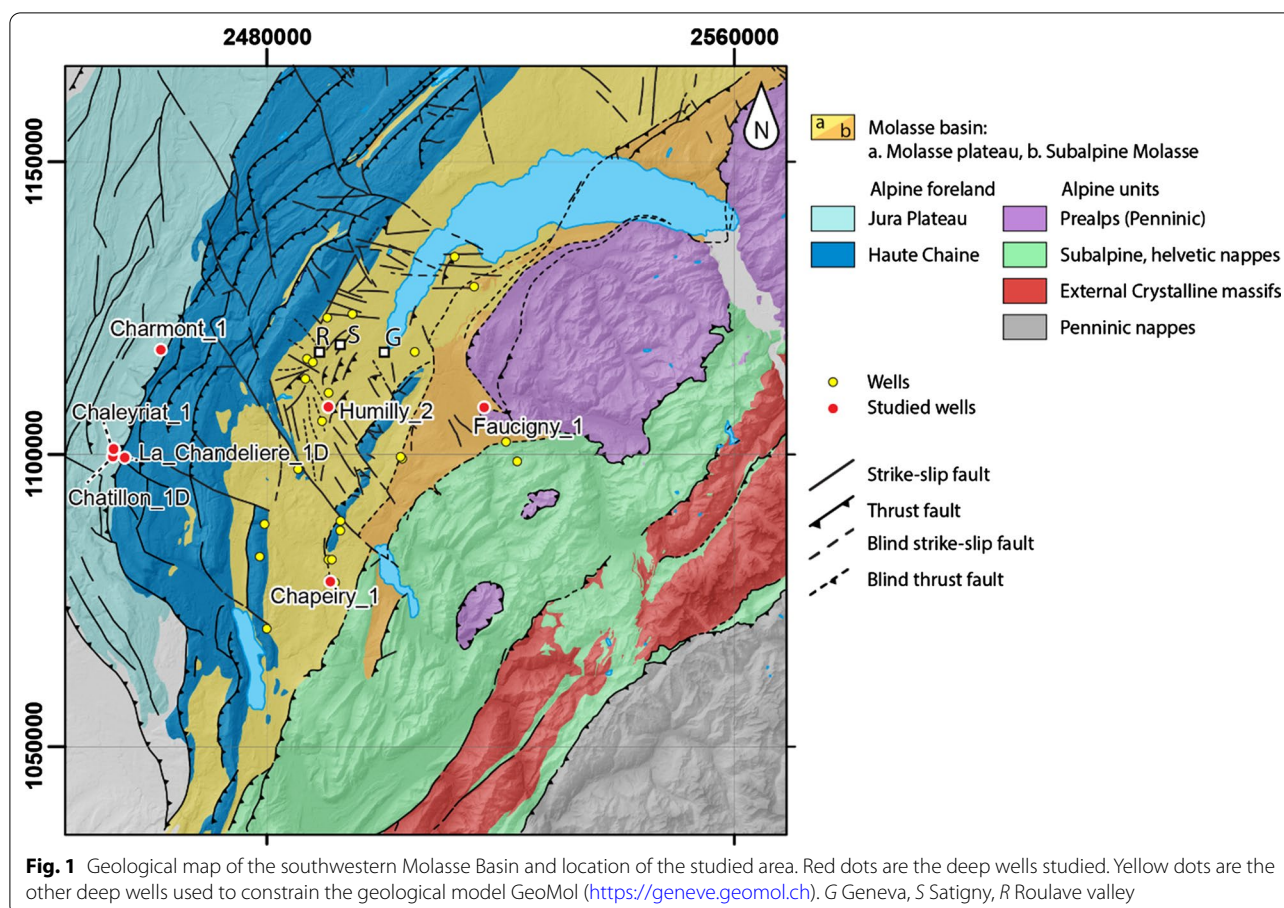
Over the last 10 years, unconventional hydrocarbon exploration and production arising from the U.S.A. renewed the interest in petroleum systems in Europe (Burri 2010; Burri et al. 2011; Littke et al. 2011; IEA 2015). So far, however, few studies considered the North Alpine Foreland Basin as a potential unconventional target (Chew 2010; Leu and Gautschi 2014). The recent discovery of a tight gas accumulation in Paleozoic rocks, encountered in Switzerland in the Noville-1 well (Leu 2012), provided new insight into unconventional resources in Switzerland. A Mesozoic marine formation referred as the Posidonia Shale (known also as Shistes Carton in near France) from the Lower Jurassic (Lias) is typically considered to represent the source rock

for conventional hydrocarbon accumulations being also associated with potential shale gas or shale oil unconventional resources (Chew 2010; Leu 2012; Leu and Gautschi 2014; Bruns et al. 2016). Additionally, the Paleozoic sequence, which remains insufficiently studied due to the lack of data is typically considered containing two potential source rock intervals, represented by the Permian (Autunian) lacustrine shales and the Carboniferous coal beds (Leu 2012; Izart et al. 2016; Pullan and Berry 2019).

The present study provides a first regional evaluation of the source rocks and related hydrocarbon generation potential in the southwestern North Alpine Foreland Basin (hereafter referred to as the Geneva Basin) and thus contributes to the overall risk assessment associated with the ongoing geothermal exploration activities in this region (Moscariello et al. 2020a). This work will present a quantitative evaluation of the potential source rocks based on new organic geochemical data measured on core and cutting samples from deep boreholes as well as bitumen and gas samples in both the Geneva and surrounding French area (Fig. 1). Finally, this study gives first insights on the risk that these source rocks represent for geothermal exploration.

2 Geological settings and petroleum system

The southwestern North Alpine Foreland Basin (NAFB) forms an asymmetric basin made of a thick Cenozoic, Mesozoic and Late Paleozoic (Carboniferous to Permian) sedimentary cover (3000–5000 m of sediments) which overlays the Variscan crystalline basement gently dipping to the S-SE. Our study area, namely the Geneva Basin, is a low relief area delimited by the Jura toward the NW, forming an arcuate fold-and-thrust belt and by the Alpine units toward the SE, forming a nappe stack (Fig. 1). The Geneva Basin developed over a crystalline basement resulting from the Variscan orogeny (Matte 2001). The orogenic collapse of the Variscan belt created a series of Carboniferous to Permian NE-SW oriented grabens in NW Europe (McCann et al. 2006; Madritsch et al. 2018). In the Geneva Basin, the stratigraphic succession extends from the Late Carboniferous to Quaternary (Fig. 2). The oldest Paleozoic sedimentary units do not crop out in the basin but have been drilled by several wells and are described in the literature (Charollais et al. 2007; Gorin et al. 1993; Signer and Gorin 1995; Sommaruga et al. 2012). The Late Carboniferous (Westphalian—Stephanian) is marked by the deposition of clastic sediments containing coal beds and dark shales in SW-NE oriented grabens and relatively small



confined basins. In the studied area, the Permian sequence has not even been encountered in the deepest exploration wells. However, it is inferred to be present at depth based on seismo-stratigraphy (Moscariello 2019) and on oil geochemistry (Pullan and Berry 2019) pointing out its limited lateral extension. Moreover, Pullan and Berry (2019) interpreted the Paleozoic succession of the wells located in the Jura region as part of the Permian sequence. No exact biostratigraphic dating is available for the Paleozoic sequences drilled at depth, but in the well reports, the Paleozoic units are consequently considered as Stephanian (Carboniferous) to Stephano-Autunian (Permo-Carboniferous) based on pollens. We hereafter apply these ages.

The Triassic period is marked by the deposition of continental to shallow marine sediments in an epicontinental sea environment. The Lower Triassic (Buntsandstein) is characterized by the deposition of sandstone. It is overlain by Middle Triassic carbonates and dolomites (Muschelkalk) and a thick sequence of evaporites (Keuper) representing an important décollement layer accommodating the shortening of the foreland basin and the Jura (Sommaruga et al. 2017). A marine transgression in the Lower Jurassic (Lias) led to the deposition of distal

marls and shales. During this period, worldwide oceanic anoxic condition improved preservation of organic matter-rich levels during the so-called Toarcian Oceanic Anoxic Event (T-OAE; Jenkyns 1988); these source rocks are widespread in northwestern and central Europe and also occur in the Mediterranean region (Baudin et al. 1990; Song et al. 2015). Depositional environment then evolved to shallower marine conditions when limestones and carbonaceous shales were deposited from the Middle to Upper Jurassic (Dogger and Malm). The Lower Cretaceous is marked by carbonate platform deposits with bioclastic limestone, whereas the Upper Cretaceous is missing. A major subaerial erosional surface affects the top of the Lower Cretaceous. It is associated with the development of karsts, filled by oxidized continental deposits (known as the siderolitic facies) and is attributed to the Late Eocene. Oligocene to Late Miocene siliciclastic deposits of marine and continental origin form the Molasse wedge above the Mesozoic series. The Subalpine Molasse, involved in a series of imbricated thrust sheets, is composed of sandstones and marlstones originated in either marine or continental freshwater depositional environment, while the rest of the Molasse (Molasse

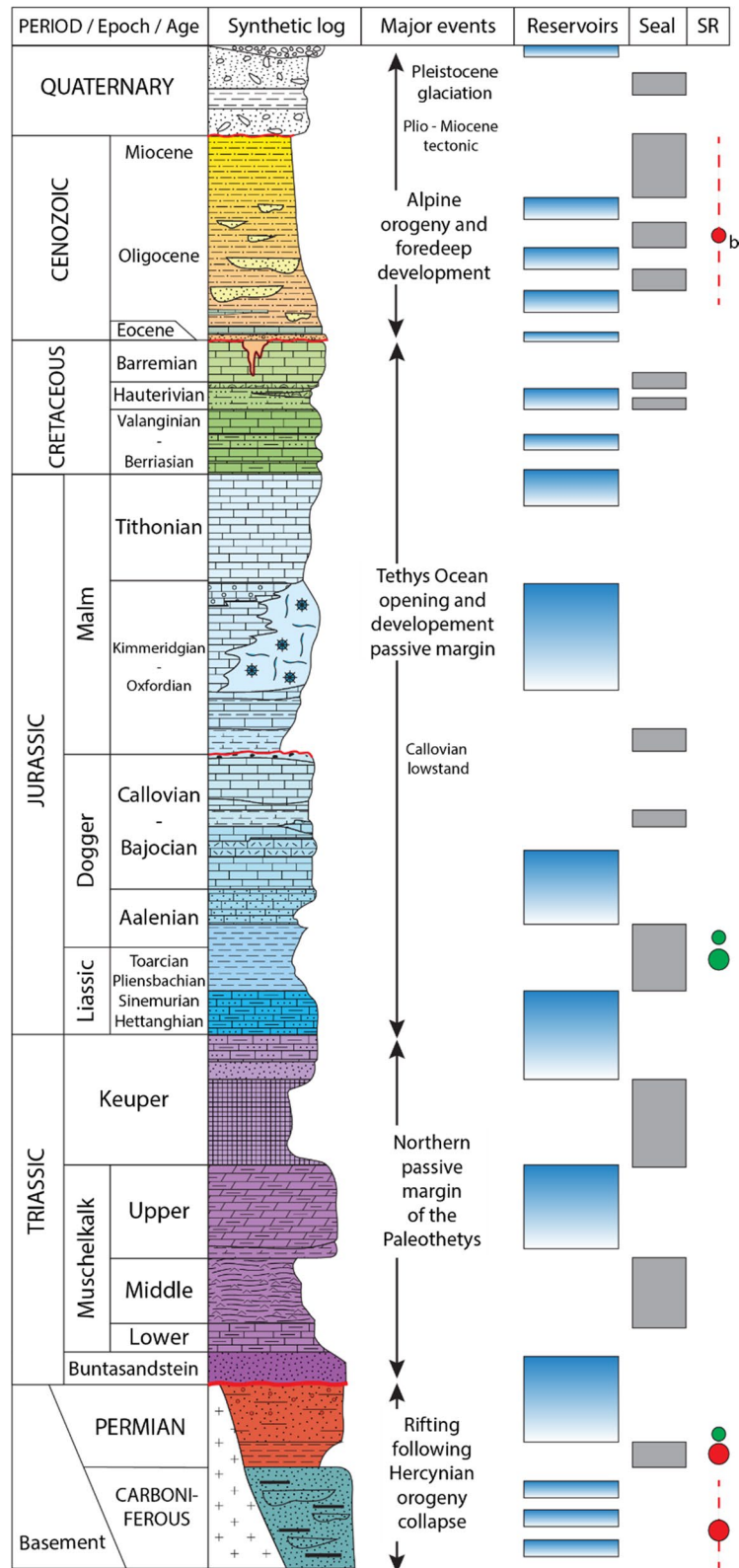


Fig. 2 Synthetic stratigraphic log of the southwestern Molasse Basin (based on well records and Leu 2012) with indication of potential reservoirs, seals and hydrocarbon source rocks (SR). Triassic and Jurassic nomenclature includes stratigraphic subdivisions commonly used in the Swiss Plateau. SR large circle: major SR; small circle: minor SR; green: oil; red: gas; b: biogenic

plateau in Fig. 1) mostly consists of clastic sediments of continental origin.

In Switzerland, several source rocks have been identified (Leu 2008, 2012) (Fig. 2) including the Carboniferous terrigenous organic matter, the Permian (Autunian) lacustrine shale and the Lower Jurassic (Toarcian) Posidonia marine shales. The Mesozoic-Cenozoic stratigraphic succession containing alternation of carbonates, marlstones, shales and other clastic layers offers several couples of reservoir and seal across the entire North Alpine Foreland basin specifically in the Jurassic/Cretaceous series that are currently under exploration for geothermal purposes as well (Chevalier et al. 2010; Leu 2012). In the Geneva Basin, both the Upper Jurassic Kimmeridgian reefs and the Lower Cretaceous bioclastic limestones form the two principal reservoir targets for geothermal district heating. However, several oil and gas shows have been reported during the drilling of the reservoir formations (Leu 2012). Oil shows in the Jura area most probably originated from the Permian Autunian shales (Pulian and Berry 2019). Geochemical data of several gas seeps on the Swiss Plateau evidenced a thermogenic origin for the gases, derived from several potential source rocks (Carboniferous, Mesozoic and Tertiary; see synthesis in Leu 2012). Even though oil seeps in the Geneva Basin have been known for a long time and even exploited since the nineteenth century (Lagatola, 1932), the origin of the hydrocarbons remained poorly constrained.

3 Materials and methods

3.1 Samples

A total of 277 rock samples were collected from 7 deep wells located in and around the southwestern termination of the Geneva Basin (Fig. 1). All samples are hereafter called by the well name and the depth below the well head (measured depth or MD). The location of the Humilly-2 well in the center of our study area, as well as its rather complete stratigraphic succession makes it a natural reference well in which 188 samples including 139 cuttings and 49 core fragments have been analyzed along the complete section, with a particularly higher sampling rate within the Toarcian layers (Appendix 1, Fig. 3, 4). This high sampling rate along the entire stratigraphic succession allowed recognition of organic-rich levels.

From the 6 other wells (Chapeiry-1, Faucigny-1, La Chandelière, Chatillon-1D, Charmont-1, Chaleyriat-1), a total amount of 89 samples (44 cuttings and 45 core fragments) has been collected mostly focusing on the Toarcian or Liassic sections and the Carboniferous (Appendix 1). The Toarcian *sensu stricto* was recognized

in the Humilly-2, Chaleyriat-1 and La Chandelière wells based on paleontological data. In the Faucigny-1 and Chapeiry-1 wells, no paleontological data allowed us to identify the Toarcian with confidence. Thus, both Upper Lias and sometimes Lower Lias were sampled (based on their lithology) and analyzed in order to confirm the presence of organic-rich material and its maturity. A total of 22 samples was collected for the Lias and 10 for the Carboniferous in these 6 wells.

The Toarcian in Humilly-2 is made of 8 m (2232–2240 m) of bituminous dark-brown to black marls and shales. In the Chapeiry-1 and Faucigny-1 wells, the Upper Lias is marked by black marls intercalated with silty to shaly limestones. In the La Chandelière and Chaleyriat-1 wells, located in the Jura region, the Toarcian consists of dark-grey silty to shaly limestone (Fig. 3).

The Carboniferous drilled in the Humilly-2 well consists of 3 m-thick fluvial sandstones and microconglomerates containing thin dark shales and coaly intercalations. In the Jura region, the Carboniferous is sometimes present (Chaleyriat-1, Charmont-1, Chatillon-1D) or absent (La Chandelière). It is represented by a thick sequence of coarse- to fine-grained sandstones alternating with micaceous mudstones and various thin coal beds of Stephanian age (Upper Carboniferous).

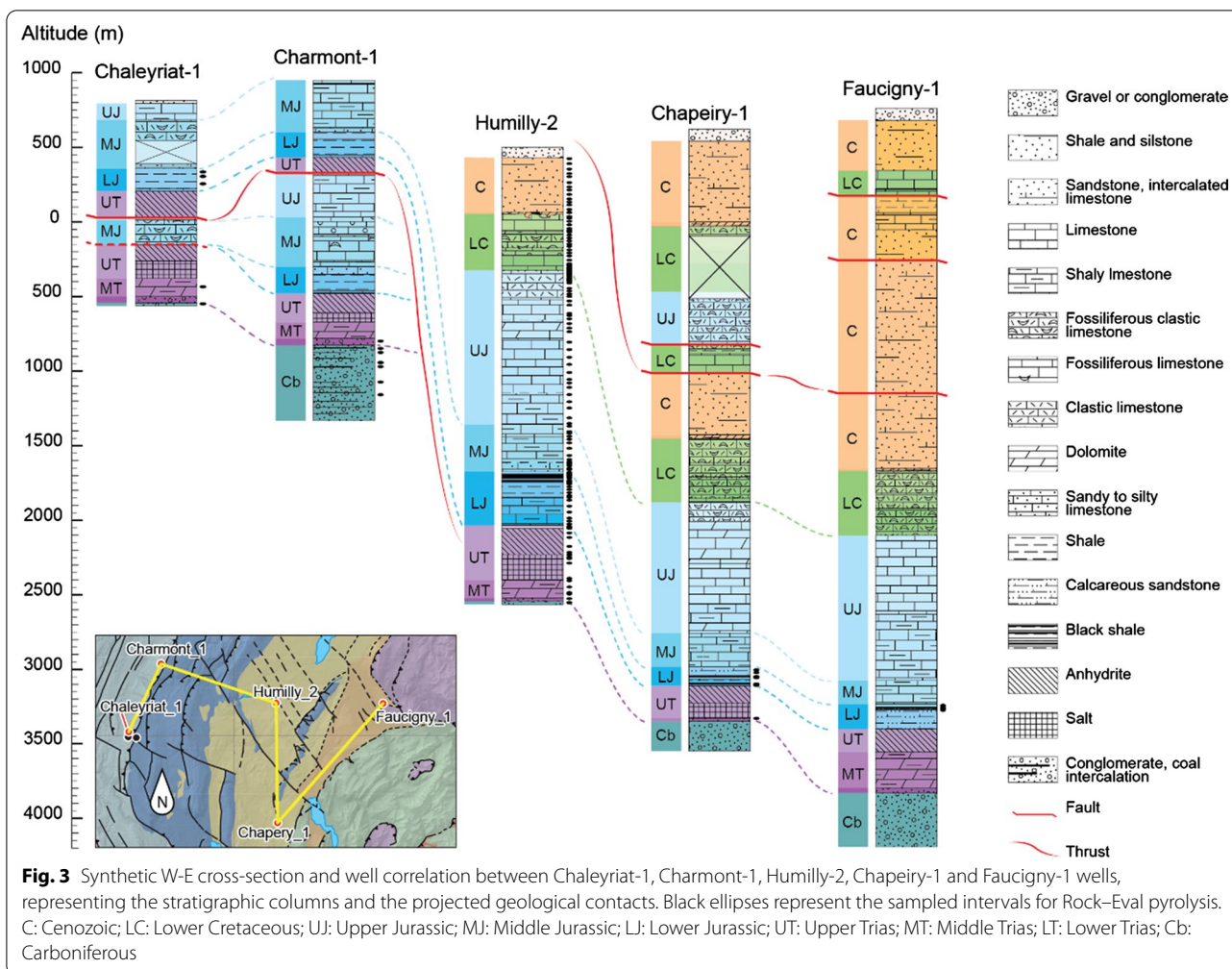
A synthetic W-E cross-section showing the correlation between 5 of the 7 wells analyzed is shown in Fig. 3 and displays the sampled intervals in the stratigraphic columns.

In addition to these source-rocks, we sampled bitumen naturally seeping from the Molasse sandstones, inside an old mining gallery along the Roulave stream. We also sampled gas and bitumen retrieved at the well-head of a ca. 80 m deep borehole drilled for heat-probe installation in Satigny, a village located 9 km West of Geneva (S in Fig. 1). It is noteworthy that the gas and bitumen in the Satigny borehole reached the well-head when the drilling reached the depth of 80 m, within the Oligocene Molasse deposits.

3.2 Methods

3.2.1 Rock-Eval pyrolysis and vitrinite reflectance

In order to identify the type and maturity of the organic matter (OM) contained in the source rocks, 28 samples of the Humilly-2 well and 32 samples from Liassic and Carboniferous sections and wells were selected for organic geochemical and petrographic analyses. Depending on the OM content, 2 to 50 mg of dried and powdered bulk rocks were used for Rock-Eval pyrolysis. Analyses were performed on a Rock-Eval 6 following procedures described by Espitalié et al. (1977) and Behar et al. (2001) to obtain: total organic carbon (TOC, wt %), S1 (mg HC/g rock), S2 (mg HC/g rock), S3 (mg CO₂/g), Hydrogen



Index (HI, mg/g TOC), Oxygen Index (OI, mg CO₂/g TOC), and T_{max} (°C). Results are given in Tables 1 and 2 for the Liassic and Carboniferous sample respectively.

Vitrinite reflectance (VRr) was measured on 15 samples (Table 3) under oil immersion at 500 × magnification using a Zeiss Axio Imager microscope. A leuco-sapphire (0.592%) mineral standard was used for calibration, except for some highly mature samples, for which a gallium gadolinium garnet (1.70%) was used. Sample preparation followed the guidelines described by Taylor et al. (1998). On some samples bitumen reflectance (BRr) was measured and converted to equivalent vitrinite reflectance using correlations published by Landis and Castaño (1995) and Schoenherr et al. (2007). Details of the analytical procedure are described in Bou Daher et al. (2015).

3.2.2 Organic geochemistry: GC-MS

The molecular organic geochemical composition of saturated hydrocarbons extracted from 12 rock samples, both from the Toarcian and the Carboniferous (Table 4) was

analyzed by gas chromatography (GC) and gas chromatography mass spectrometry (GC-MS), following the analytical protocol described in Bou Daher et al. (2015). Identification of biomarkers in the aliphatic fractions of the different samples was done by comparison with published mass spectra (Peters et al. 2005). In order to link the source-rocks to the oil and gas shows at surface and shallow depth, the aliphatic fractions of two bitumen samples taken in the Roulave stream (R in Fig. 1) and the Satigny borehole was analyzed using GC-MS.

Moreover, the geochemical and stable isotopic composition of two gas samples originating from an unexpected gas pocket encountered at a depth of ca. 70 m in the Satigny well, 9 km west of Geneva (Fig. 1) was analysed at BGR Hannover. Two samples, SAT1 and SAT2, were collected from the well head at near atmospheric pressure using a syringe and injected into a 20 mL head-space vial with a septum lined crimp cap and filled with helium. Sample SAT1 was filled with 100 µL of gas and 200 µL in sample SAT2. The injected gas volume was 100

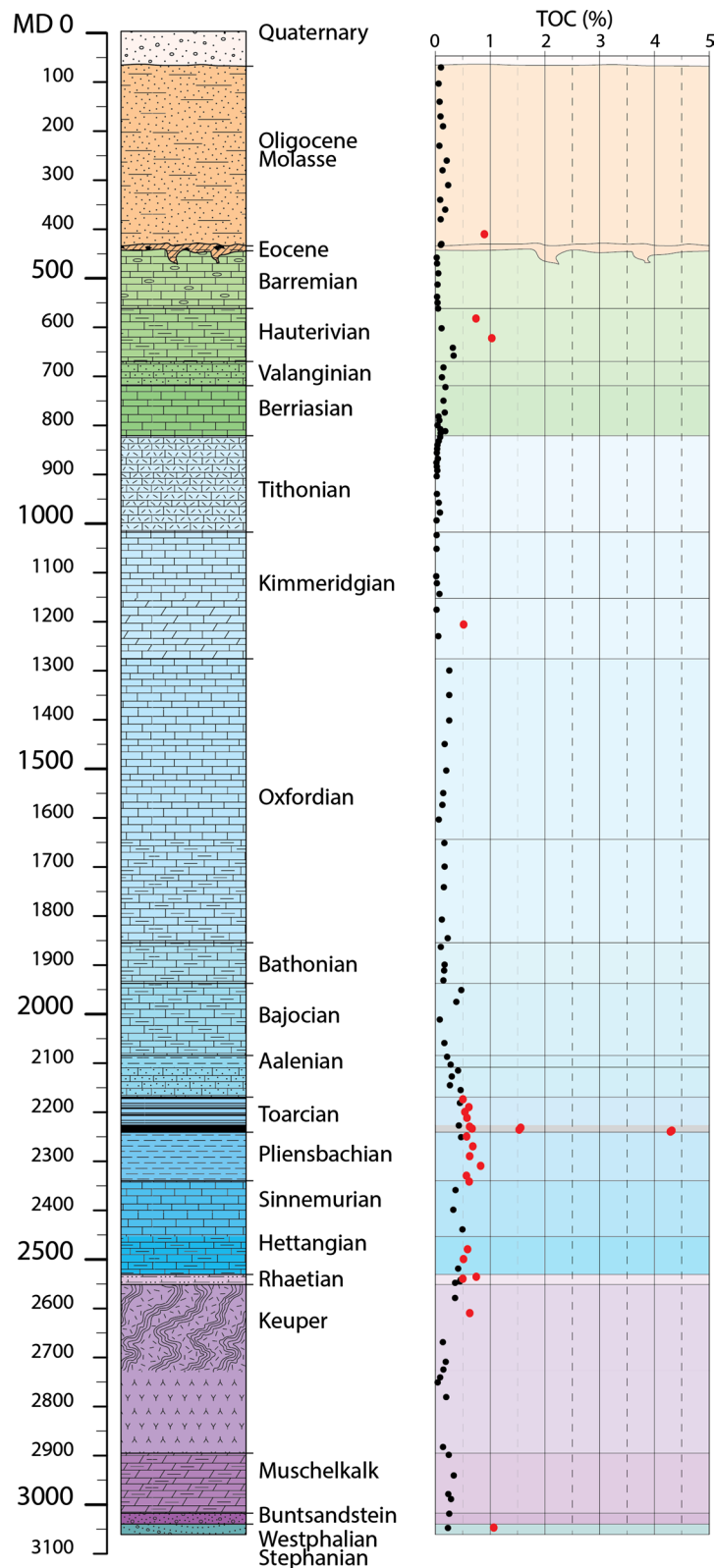


Fig. 4 Stratigraphic log of the Humilly-2 well (see Fig. 1 for location) with TOC values measured on cutting samples across the entire stratigraphic section. Red dots highlight samples where TOC > 0.5%

Table 1 Rock-Eval pyrolysis results of samples from Liassic sections in the studied wells

Wells	Depth (MD)	Stratigraphic age	TOC (%)	MINC (%)	S1 (mg HC/g)	S2 (mg HC/g)	S3 (mg CO ₂ /g)	HI (mg/g TOC)	OI (mg CO ₂ /g TOC)	Tmax (°C)	PI	
Humilly-2	2174	Toarcian	0.50	3.23	0.06	0.67	0.28	133	56	435	0.08	
Humilly-2	2182		0.45	3.67	0.08	0.60	0.18	133	40	434	0.12	
Humilly-2	2190		0.61	1.77	0.14	0.80	0.26	132	43	434	0.15	
Humilly-2	2200		0.54	4.09	0.08	0.51	0.26	94	49	433	0.14	
Humilly-2	2212		0.58	3.24	0.07	0.56	0.25	97	43	437	0.11	
Humilly-2	2228		(0.43)	4.95	0.06	0.64	0.23	149	54	435	0.09	
Humilly-2	2230		0.62	4.44	0.07	0.76	0.23	121	36	439	0.08	
Humilly-2	2232		1.56	5.11	0.38	3.49	0.29	224	19	438	0.10	
Humilly-2	2234		0.67	5.00	0.14	1.06	0.25	158	37	437	0.12	
Humilly-2	2236		1.53	5.21	0.37	4.93	0.27	322	18	441	0.07	
Humilly-2	2238		4.32	5.24	1.41	21.80	0.63	505	15	443	0.06	
Humilly-2	2240		4.29	4.45	1.18	20.65	0.65	481	15	441	0.05	
Humilly-2	2250	Pliensbachian	0.57	5.76	0.08	0.69	0.19	120	34	441	0.10	
Humilly-2	2252		0.47	4.65	0.10	0.62	0.50	132	107	439	0.14	
Humilly-2	2270		0.68	2.58	0.06	0.56	0.19	82	28	438	0.10	
Humilly-2	2290		0.63	2.13	0.07	0.89	0.25	142	40	443	0.07	
Humilly-2	2310		0.83	2.13	0.08	0.95	0.41	115	49	444	0.08	
Humilly-2	2330		0.57	2.08	0.07	0.66	0.26	117	47	440	0.10	
Humilly-2	2342		0.62	3.14	0.05	0.53	0.25	86	41	441	0.09	
Humilly-2	2360		(0.37)	6.03	0.04	0.27	0.21	73	58	438	0.13	
Humilly-2	2400		(0.33)	8.20	0.05	0.26	0.20	80	61	440	0.16	
Humilly-2	2440		0.49	4.85	0.05	0.48	0.26	97	53	440	0.09	
Humilly-2	2480	Sinemurian	0.59	5.74	0.12	0.57	0.29	97	50	441	0.17	
Humilly-2	2500		0.51	5.35	0.06	0.46	0.23	89	44	442	0.12	
Humilly-2	2520		(0.42)	6.17	0.04	0.35	0.24	85	57	439	0.10	
Faucigny-1	4001.0		Upper Lias	0.93	4.82	0.11	0.82	0.20	88	21	529	0.12
Faucigny-1	4007.0			1.02	5.04	0.13	0.75	0.26	74	26	518	0.15
Faucigny-1	4015.0			0.93	4.44	0.10	0.84	0.12	90	13	526	0.11
Faucigny-1	4020.0			1.03	4.83	0.10	0.76	0.19	74	19	527	0.12
Faucigny-1	4026.0			1.59	5.04	0.21	1.07	1.00	68	63	527	0.16
Faucigny-1	4027.0			1.56	4.24	0.19	0.59	0.22	38	14	515	0.24
Faucigny-1	4035.0			0.94	4.73	0.06	0.39	0.15	42	16	560	0.13

Table 1 (continued)

Wells	Depth (MD)	Stratigraphic age	TOC (%)	MINC (%)	S1 (mg HC/g)	S2 (mg HC/g)	S3 (mg CO ₂ /g)	HI (mg /g TOC)	OI (mg CO ₂ /g TOC)	Tmax (°C)	PI
Chapeiry-1	3624.0	Upper Lias	(0.35)	5.40	0.02	0.14	0.20	39	55	438	0.13
Chapeiry-1	3642.0		(0.32)	5.76	0.01	0.08	0.21	26	64	439	0.11
Chapeiry-1	3669.0		3.52	4.59	1.23	7.04	0.52	200	15	446	0.15
Chapeiry-1	3670.0		2.21	7.05	1.01	3.75	0.68	170	31	445	0.21
Chapeiry-1	3677.0		0.63	3.10	0.02	0.14	0.66	22	106	436	0.13
Chapeiry-1	3719.4	Lower Lias	1.46	2.69	0.30	1.74	0.40	119	28	445	0.15
Chapeiry-1	3719.8		(0.33)	10.17	0.33	0.30	0.25	89	76	426	0.52
Chapeiry-1	3720.9		1.39	5.03	2.21	4.12	0.57	297	41	410	0.35
Chapeiry-1	3722.7		3.29	0.20	3.34	6.52	0.36	198	11	442	0.34
Chapeiry-1	3728.8		4.15	0.58	3.05	6.48	0.53	156	13	442	0.32
Chaleyriat-1	480	Toarcian	0.97	1.71	0.22	2.08	0.33	215	34	428	0.10
Chaleyriat-1	510		0.79	1.35	0.04	1.23	0.31	157	39	435	0.03
Chaleyriat-1	560		0.76	1.16	0.04	0.93	0.48	121	63	431	0.04
La Chandelière	1130.0	Toarcian	(0.21)	5.83	0.05	0.30	0.64	144	310	427	0.14
La Chandelière	1150.0		(0.30)	5.63	0.05	0.47	0.54	156	180	432	0.10

Samples between brackets contain less than 0.5% of TOC and are not plotted in the graphs

Table 2 Rock–Eval pyrolysis results of Carboniferous sections in the studied wells

Wells	Depth	Stratigraphic age	TOC (%)	S1 (mg HC/g)	S2a (mg HC/g)	S3 (mg CO ₂ /g)	HI (mg HC/g TOC)	OI (mg CO ₂ /g TOC)	Tmax (°C)	PI
Humilly-2	3039.8	Carboniferous	1.12	0.10	0.85	0.15	76	13	449	0.11
Humilly-2	3040.7		1.11	0.09	0.61	0.16	55	15	465	0.13
Humilly-2	3049		0.23	0.11	0.37	1.08	161	470	461	0.23
La Chandelière	1562.1	Carboniferous	0.11	0.04	0.53	0.38	467	337	545	0.07
Chaleyriat-1	1365.0	Carboniferous	0.88	0.03	0.45	1.21	51	137	514	0.06
Charmont-1	1798.0	Carboniferous	5.10	0.30	4.69	0.51	92	10	430	0.06
Charmont-1	1825.0		22.57	1.50	44.25	5.63	196	25	435	0.03
Charmont-1	1892.0		31.81	2.28	69.39	8.50	218	27	433	0.03
Charmont-1	1894.0		54.85	3.88	126.84	5.91	231	11	435	0.03
Charmont-1	1920.0		16.09	0.71	21.59	3.67	134	23	437	0.03
Charmont-1	2023.0		7.19	0.33	6.43	1.28	89	18	460	0.05
Charmont-1	2108.5		57.33	6.36	125.66	6.19	219	11	450	0.05
Chatillon-1D	1578.5	Carboniferous	8.24	0.52	7.78	0.64	94	8	444	0.06

μL for sample SAT1 and 200 μL for sample SAT2. The molecular gas composition was analysed using a Refinery Gas Analyzer (RGA; Joint Analytical Systems GmbH) that quantifies the light-volatile hydrocarbons methane to hexane and the permanent gases helium, hydrogen, oxygen, nitrogen, carbon monoxide and carbon dioxide. The stable carbon and hydrogen isotope composition was analyzed by gas chromatography-isotope ratio monitoring mass spectrometry (GC-IRMS) using an Agilent 6890 gas chromatograph, coupled to a Thermo Fisher MAT 253 mass spectrometer. The stable isotope composition is reported using the delta notation relative to Vienna Pee Dee Belemnite (VPDB) standard for carbon and Vienna Standard Mean Ocean Water (VSMOW) standard for hydrogen. Details on the molecular and stable isotope analysis of gas samples are provided in Weniger et al. (2019).

4 Results

4.1 Rock–Eval pyrolysis and vitrinite reflectance

Rock–Eval pyrolysis results are presented in Figs. 4 and 5 and in Tables 1 and 2 for the Liassic and Carboniferous samples, respectively. Samples containing less than 0.50% wt TOC are kept in the tables but not plotted in the graphs.

4.1.1 Lias

TOC content ranges between 0.21 and 4.32% with a mean value of 1.1%. The highest value is observed in the Toarcian of Humilly-2 well at a depth of 2238 m. Free hydrocarbons (S1 values) are low and vary between 0.01 and 3.34 mg/g with an average of 0.38 mg/g. The highest S1 value is observed in the lower Lias of Chapeiry-1 well at a

depth of 3722.7 m. Hydrocarbon generation potential (S2 values) varies between 0.08 and 21.8 mg/g with an average of 2.22 mg/g. Highest S2 values are recorded in the lowermost Toarcian samples of Humilly-2 well. T_{max} values vary between 320 and 560 °C and have an average of 447 °C. Except for Faucigny-1 where T_{max} exceeds 500 °C, the other well samples reveal T_{max} values between 410 and 446 °C. HI values fluctuate between 22 and 505 mg/g TOC with an average value of 137 mg/g TOC. OI values vary between 11 and 310 mg CO₂/g TOC with an average of 50 mg CO₂/g TOC. High HI values seem to be correlated with high TOC content, except for the Faucigny-1 well, where samples are overmature and have lost their hydrocarbon generation potential (Table 3), whereas OI values tend to increase at low TOC content. These trends may be linked with a mineral matrix effect (MME) that tends to increase OI (especially for carbonated samples) and decrease HI (for shale samples) in low TOC samples (Espitalié et al, 1984; 1985; Grohmann et al, 2019).

Vitrinite reflectance in Humilly-2 and Chapeiry-1 wells vary from 0.72 to 0.77% with a standard deviation between 0.04 to 0.07 (Table 3). In the Faucigny-1 well, no vitrinite was found however bitumen reflectance was measured between 2.07 to 2.22% (Table 3). Such bitumen reflectance reflects an equivalent vitrinite reflectance from 2.22 to 2.41% according to Landis and Castaño (1995) and Schoenherr et al. (2007).

4.1.2 Carboniferous

TOC content ranges between 0.1 and 57.33% with a mean value of 15.9%, the highest value being found in Charmont-1 well at a depth of 2108.50 m. S1 values vary between 0.03 and 6.36 mg/g with an

Table 3 Vitrinite reflectance results of the Liassic and Carboniferous sections in the studied wells

	Well	Sample	TOC (%)	Tmax (°C)	VRr (%)	Std dev	Rb (%)	Nbr vitrinites measured	
Lias	Humilly-2	HU2 -2232	1.56	438	0.72	0.05	-	13	
		HU2—2236	1.53	441	0.74	0.06	-	14	
		HU2—2238	4.32	443	0.74	0.06	-	31	
		HU2—2240	4.29	441	0.74	0.07	-	33	
	Chapeiry-1	CHY—3669	3.52	446	0.76	0.06	-	9	
		CHY—3720.9	1.39	410	0.77	0.04	-	13	
		CHY—3722.7	3.29	442	0.72	0.04	-	13	
	Faucigny-1	FAY—4020	1.03	527	2.21–2.28*	0.14	2.07	22	
		FAY—4026	1.59	527	2.35–2.41*	0.10	2.22	39	
		FAY—4027	1.56	515	2.22–2.29*	0.12	2.09	47	
	Carboniferous	Humilly-2	HU2 – 3039.8	1.12	449	1.14	0.07	-	50
		Charmont-1	CHT—1892	31.81	433	0.60	0.03	-	100
CHT—1894			54.85	435	0.64	0.02	-	100	
CHT—2108.5			57.33	450	0.79	0.03	-	100	
Chatillon-1D		CTL1D—1578.5	8.24	444	0.76	0.03	-	100	
La Chandelière		LCD—1553.2	n/a	n/a	0.75	0.04	-	16	

*Vitrinite reflectance ranges calculated from bitumen reflectance according to Landis and Castaño (1995) and Schoenherr et al. (2007)

average of 1.25 mg/g. S2 values range between 0.37 and 126.84 mg/g with a mean value of 31.5 mg/g. Highest S2 values at 125.66 and 126.84 mg/g are recorded in organic-rich coals of Charmont-1 well (TOC of respectively 57.33 and 54.85%). T_{max} values vary between 430 and 545 °C and have an average of 455 °C. Except for the coal-bearing sandstones of La Chandelière and Chaleyriat-1 well where T_{max} respectively reaches 545 °C and 514 °C, the other well samples reveal T_{max} values between 430 and 465 °C. HI values vary between 51 and 467 mg/g C. The highest HI value is found in the coal-bearing sandstone of La Chandelière well, but it displays very low TOC (0.1%) and a high T_{max} (545 °C) indicating that this value is not reliable and will not be further discussed. Except for this sample, Carboniferous samples are characterized by HI values between 51 and 231 mg/g C with a mean value of 135 mg/g TOC. OI values vary between 8 and 470 mg CO₂/g TOC with an average of 85 mg CO₂/g TOC. Pure coals display low OI values between 8 and 27 mg CO₂/g TOC. Except for the three samples composed of coal-bearing sandstones (Humilly-2 at 3049 m depth; La Chandelière at 1562.1 m; Chaleyriat-1 at 1365 m), high HI values and low OI values are correlated with high TOC content.

In the Jura region (Charmont-1, Chatillon-1D and La Chandelière), vitrinite reflectance vary from 0.60 to 0.79%, with a standard deviation below 0.04 (Table 3). The highest vitrinite reflectance has been measured in the Humilly-2 well with a reflectance of 1.14%.

4.2 Chromatographic analysis

Source rock chromatograms and discussed biomarker results are presented in Figs. 6, 7 and Table 4.

4.2.1 Lias

Short-chain *n*-alkanes (<*n*-C₁₉) are predominant compared to mid- (*n*-C₂₀₋₂₆) and long-chain (>*n*-C₂₆) *n*-alkanes in almost all Jurassic samples (Fig. 6), which is typical of marine OM derived from bacteria and/or algae (Peters et al. 2005). The only exceptions are the Chapeiry-1 3720.9 and 3722.7 samples where mid-chain *n*-alkanes display very high concentrations, suggesting a significant contribution from aquatic macrophytes (Ficken et al. 2000). Sample Chapeiry-1 3722.7 is also the only one displaying a bimodal distribution of *n*-alkanes, indicating higher plant inputs. It should also be noted that samples 3720.9 and 3728.8 also display significant long-chain *n*-alkanes concentrations. The terrigenous/aquatic ratios (TAR) defined by Bourbonniere and Meyers (1996) as $[(n-C_{27} + n-C_{29} + n-C_{31}) / (n-C_{15} + n-C_{17} + n-C_{19})]$, is an indicator of the relative input of terrestrial plant versus aquatic OM. TAR values range from 0.01 to 0.44. Accordingly, values above 0.1 are only found in the Chapeiry samples (Table 4) with significant long-chain *n*-alkane concentrations, indicating higher terrestrial plant contributions.

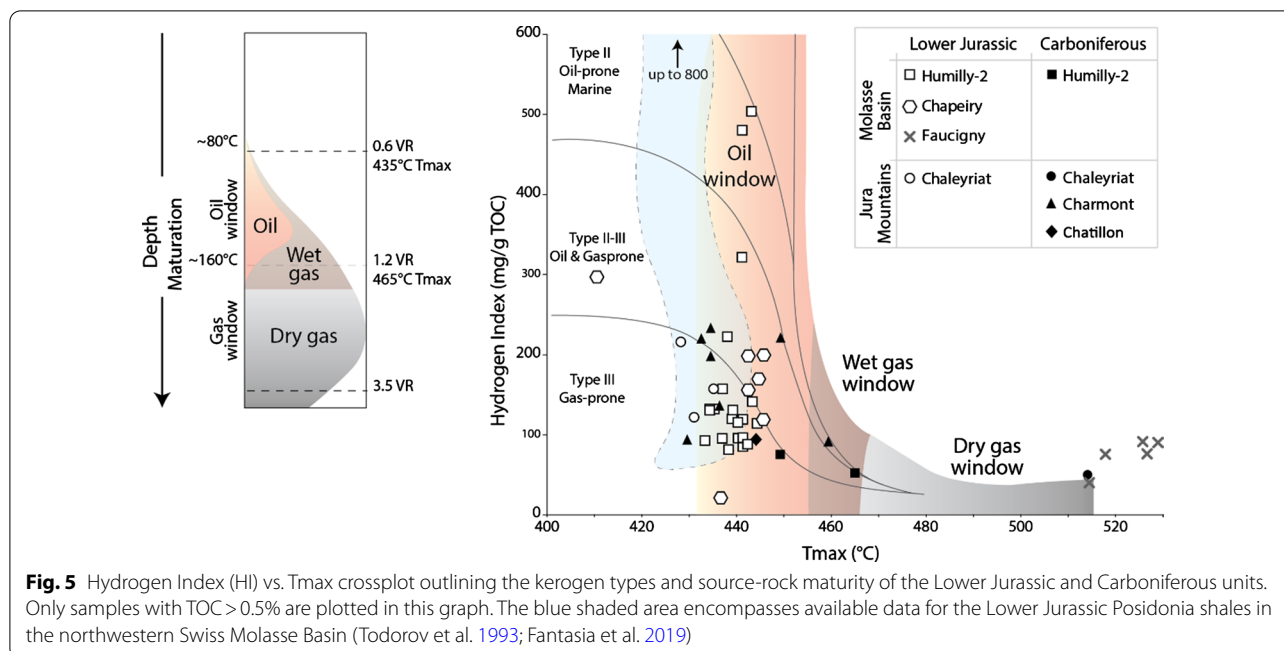
The carbon preference index (CPI₂₅₋₃₁) (Bray and Evans 1961) was calculated when possible (i.e. 4 Toarcian samples did not show the requested *n*-alkanes)

Table 4 Overview of biomarker ratios determined in this study

Well	Depth	Stratigraphic age	TOC (%)	Pr/Ph	Pr/nC17	Ph/nC18	TAR	CPI	C29 norHop/ C30 Hop	C31 Hop 225/(22R+22S)	St C27	St C28	St C29
Humilly-2	2232	Toarcian	1.56	1.94	0.38	0.33	-	-	-	-	-	-	-
Humilly-2	2236		1.53	2.06	0.83	0.63	-	-	0.34	0.58	34.69	23.79	41.52
Humilly-2	2238		4.32	1.51	0.76	0.75	0.04	1.38*	0.37	0.57	31.37	27.59	41.03
Humilly-2	2240		4.29	1.42	0.69	0.65	0.03	-	0.30	0.66	34.96	24.65	40.39
Humilly-2	3038.8	Carb	1.12	1.53	0.61	0.48	0.93	1.06	-	-	35.66	33.25	31.09
Humilly-2	3040.7		1.11	0.88	0.63	0.66	2.5	1.05	-	-	35.15	33.5	31.35
Chatillon-1D	1578.5	Carb	8.24	1.06	0.97	1.09	0.15	1.27	0.38	0.57	29.13	20.27	50.61
Charmont-1	1892	Carb	31.81	6.88	4.04	0.58	0.15	1.48*	0.87	0.58	21.46	16.35	62.19
Charmont-1	1894		54.85	6.75	2.08	0.32	0.28	1.74*	0.83	0.58	23.39	20.70	55.91
Charmont-1	2108.5		57.33	6.23	2.30	0.41	0.03	-	1.09	0.58	21.81	24.66	53.53
Chapeiry-1	3669	Toarcian	3.52	1.76	0.51	0.42	0.01	-	-	-	-	-	-
Chapeiry-1	3720.9		1.39	1.26	1.59	1.18	0.24	1.48	0.74	0.60	42.22	28.29	29.49
Chapeiry-1	3722.7		3.29	0.87	0.60	0.62	0.44	1.13	0.73	0.58	48.94	19.43	31.63
Chapeiry-1	3728.8		4.15	1.23	0.44	0.41	0.13	1.11	0.35	0.61	36.66	25.15	38.19
Roulave bitumen	Surface	-	-	0.62	3.05	40.45	0.15	-	0.31	0.57	36.04	24.38	39.58
Satigny bitumen	Surface	-	-	-	-	-	-	-	0.39	0.42	-	-	-
Satigny bitumen	Surface	-	-	-	-	-	-	-	0.31	0.5	-	-	-

Pr, pristane, Ph, phytane, TAR Terrigenous Aquatic Ratio, CPI Carbon Preference Index, Hop hopane, Str sterane

*CPI₁₅₋₂₉ value



and display values ranging from 1.1 to 1.5. When only n -C₃₂ was absent, a CPI was calculated for odd-number n -alkanes between C₂₅ and C₂₉. For Toarcian samples, the Humilly-2 2238 sample was the only one in that case and display a CPI value of 1.38. Pristane (Pr) is predominant over phytane (Ph), except for the Chapeiry-1 3722 sample, and the Pr/Ph ratios vary between 0.87 and 2.06, the lowest being associated with the Chapeiry-1 3722 sample. Pr/ n -C₁₇ ratios mostly range from 0.37 to 0.83, and Ph/ n -C₁₈ ratios from 0.33 to 0.75. The only exception is the Chapeiry-1 3722 sample showing a value of 1.6. and 1.2 for the Pr/ n -C₁₇ and Ph/ n -C₁₈ ratios, respectively. In a Pr/ n -C₁₇ vs. Ph/ n -C₁₈ diagram (Fig. 7a), all Jurassic samples plot in the mixed organic matter domain (Shanmugam 1985; Hunt 1996).

Regarding relative abundance of the C₂₇, C₂₈, and C₂₉ regular steranes, it appears that the Humilly-2 samples are all dominated by the C₂₉ (>40%) whereas the ones from the Chapeiry-1 well are dominated by the C₂₇ (>42%) except for the lowermost sample that is also dominated by the C₂₉ (38.2%). According to the distribution of these samples in a ternary diagram (Fig. 7b), the Liassic samples fall into the area typical of open marine depositional environment, except for the Chapeiry-1 3728.8 sample that plots in the coastal shallow marine domain. Furthermore, it suggests that the OM source of Jurassic samples is mostly derived from marine phytoplankton marine with variable contribution from higher land plants (Peters et al. 2005).

The C₂₉/C₃₀ hopane ratio (Peters et al. 2005) is below 1 for all the Jurassic samples. The only homohopanes found in our samples are the C₃₁ 22S and 22R. The homohopane 22S/(22S + 22R) isomerization ratio (Peters et al. 2005) is relatively high and varies between 0.57 and 0.66.

4.2.2 Carboniferous

Compared to Jurassic samples, the Carboniferous samples display higher concentrations in mid- (n -C₂₀₋₂₆) and long-chain (> n -C₂₆) n -alkanes, which indicate stronger higher plant contributions (Fig. 6). Yet, only two samples (Charmont-1 1894 and Humilly-2 3040.7) are not strictly dominated by short-chain n -alkanes. The latter samples, and the Humilly-2 3039.8 sample, display a bimodal distribution (Fig. 6f–h). While the dark shale samples from Humilly-2 show high proportions of short- (especially in 3039.8 sample) and long-chain n -alkanes, the coal sample from the Charmont-1 well displays relatively high proportions of both short- and mid-chain n -alkanes. Moreover, all the other samples from Charmont-1 (Fig. 6e) and Chatillon-1D wells (Fig. 6d) display significant contributions of mid-chain n -alkanes, but only low relative concentrations of long-chains. TAR values are generally higher than the Jurassic ones, above 0.9 (up to 2.5) in the Humilly-2 samples. This is coherent with relatively higher terrestrial plant contributions compared to the samples from the Charmont-1 and Chatillon-1D wells (Peters et al. 2005).

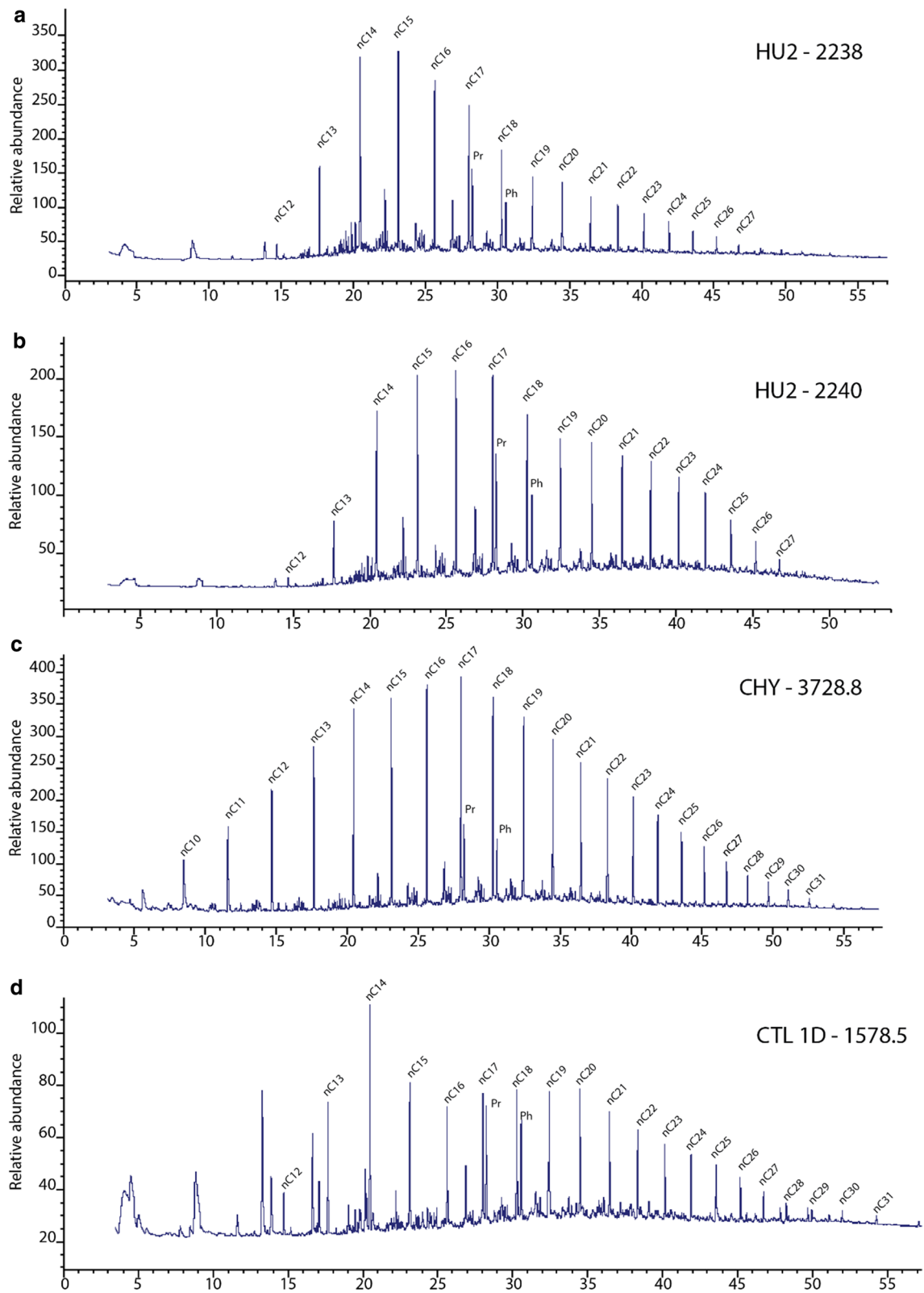


Fig. 6 Typical aliphatic fraction total ion chromatograms for the Toarcian unit of (a, b) Humilly-2 and (c) Chapeiry-1 well and the Carboniferous coal of (d) Chatillon-1D, (e, g) Charmont-1 and (g, h) Humilly-2

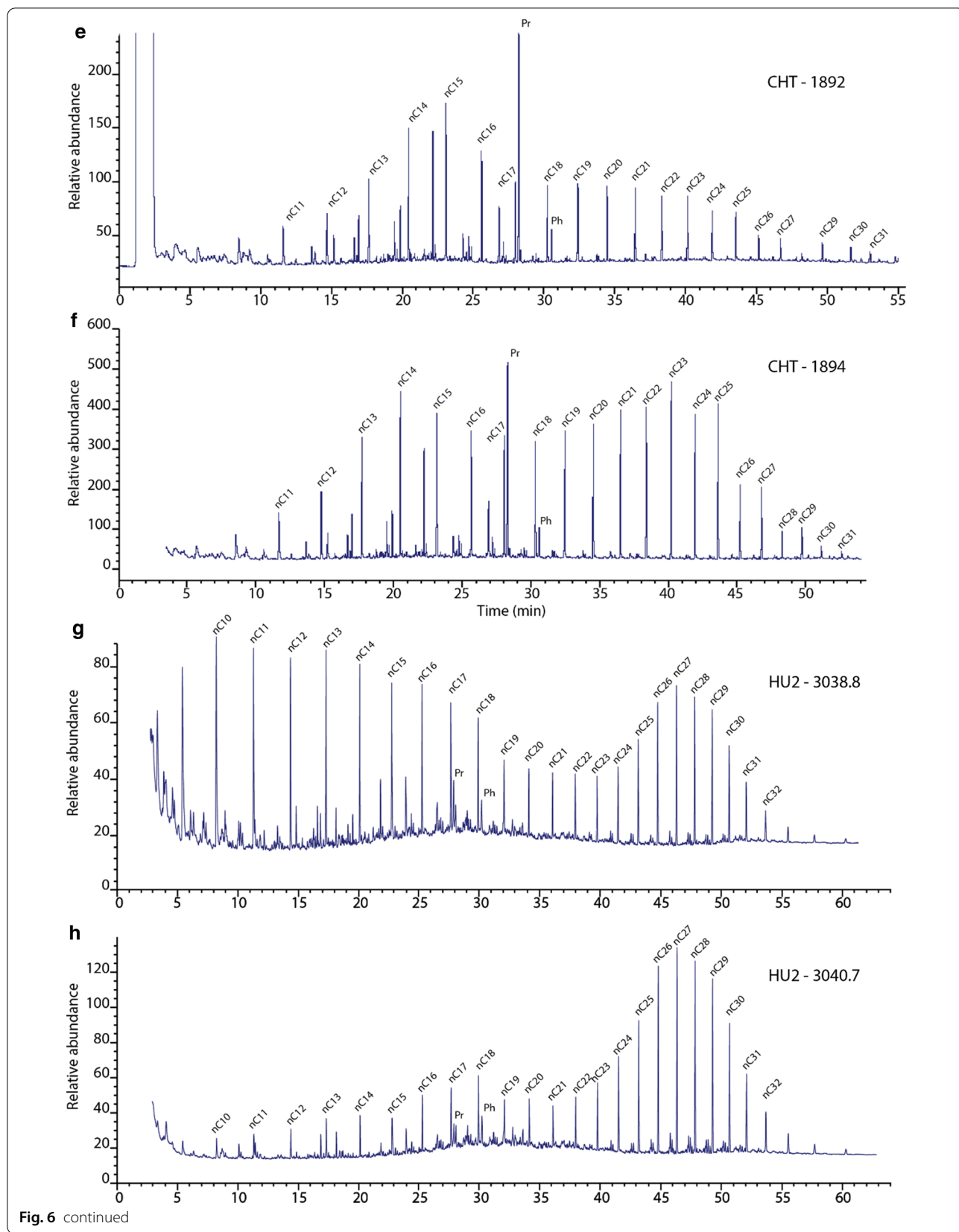
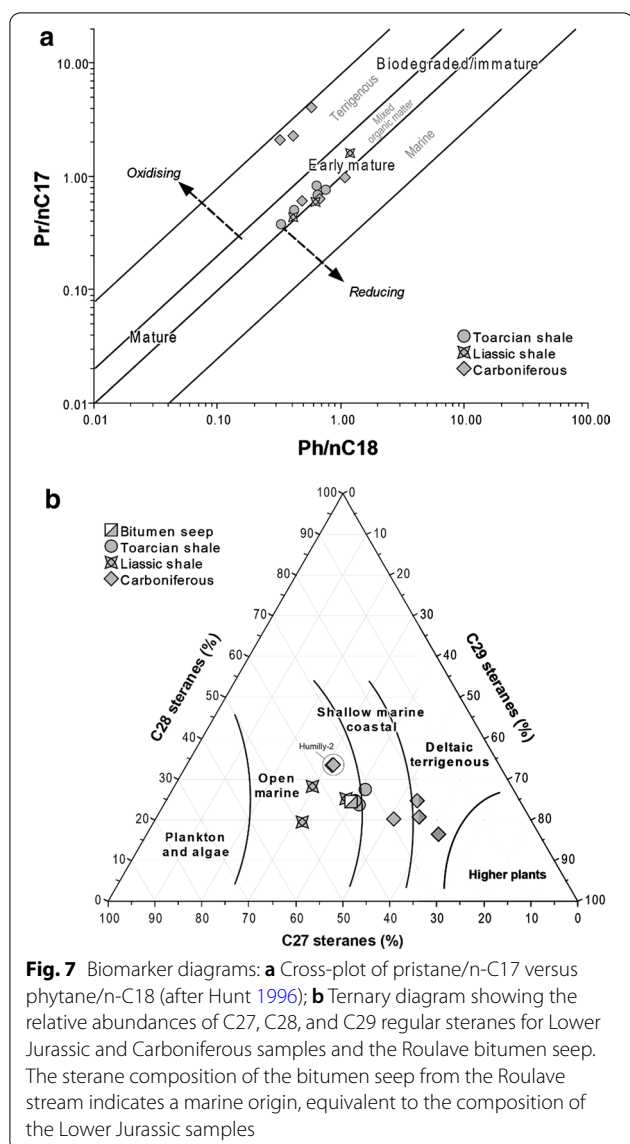


Fig. 6 continued



The carbon preference index (CPI_{25-31}) displays values ranging from 1.05 (in Humilly-2) to 1.3 (in Chatillon-1D). As $n-C_{32}$ is absent in Charmont-1 samples, the CPI_{25-29} , that was calculated instead, shows values between 1.5 and 1.7. Pristane/phytane ratios are clearly higher in Charmont-1 samples ($Pr/Ph > 6$), indicating a strong predominance of pristane. In other samples, Pr/Ph is below 1.6 and even below 1 for Humilly-2 3040.7. $Pr/n-C_{17}$ ratio ranges from 0.61 to 0.97 for Humilly-2 and Chatillon-1D samples, and between 2.08 and 4 for Charmont-1 ones. $Ph/n-C_{18}$ ratios vary from 0.32 to 1.09, the maximum being found in Chatillon-1D sample. In a $Pr/n-C_{17}$ vs. $Ph/n-C_{18}$ diagram (Fig. 7a), Carboniferous samples from the Charmont-1 well plot in the terrigenous domain, the sample Humilly-2 3039.8

in the mixed organic matter one, and the other samples in the marine domain (Hunt 1996).

Regarding the regular steranes relative abundance, it appears that Humilly-2 samples are dominated by C_{27} (>35%) whereas Charmont-1 and Chatillon-1D samples all show a dominance of C_{29} (>50%). Plotting these results in a regular sterane ternary diagram indicates that the Charmont-1 well samples were deposited in a deltaic terrigenous environment, the Chatillon-1D samples in a shallow coastal marine one, and the ones from Humilly-2 in an open marine environment (Peters et al. 2005). Moreover, it suggests that higher plant contributions are stronger for the Charmont-1 and Chatillon-1D samples compared to Humilly-2, which is contradictory with TAR values presented above. This kind of ternary diagram should in fact be interpreted with caution as the interpretation of the relationship between the relative sterane abundance and the depositional environment vs. the OM producers has not yet found consensus within the scientific community (see Peters et al. 2005 for discussion).

The C_{29}/C_{30} hopane ratio (Peters et al. 2005) ranges between 0.38 and 1.09 for the Carboniferous samples, and are all above 0.8 in the Charmont-1 samples. The homohopane $22S/(22S + 22R)$ isomerization ratio (Peters et al. 2005), calculated for C_{31} only, is around 0.58 for all the samples.

4.3 Bitumen and gas characterization

4.3.1 Bitumen

The aliphatic fraction chromatogram of the Roulave and Satigny bitumens (Fig. 8) shows a characteristic unresolved complex mixture (UCM or 'hump') typical of moderate to heavy biodegraded oil (Peters et al. 2005). Such chromatogram pattern does not allow us to determine precisely the origin of the organic matter. Still, regular steranes C_{27} , C_{28} and C_{29} have been detected (Table 4) and their relative abundance indicates a phytoplanktonic source of organic matter and suggest that the organic matter from which the bitumen originated has been deposited under open marine conditions (Fig. 7b).

4.3.2 Gas geochemistry

The gas retrieved from the shallow drilling at Satigny (Fig. 1) revealed that both samples contained hydrocarbons (C1-C6 range) and 15 to 19 vol.% air (contamination during sampling). Interestingly, the Satigny gas sample did not contain any detectable CO_2 (Table 5). The relative alkane composition of both samples is nearly identical and dominated by methane (99%), typical for a 'dry' gas (Table 5). In both samples, the alkane concentration decreases with increasing molecular weight. The mean gas dryness was calculated for

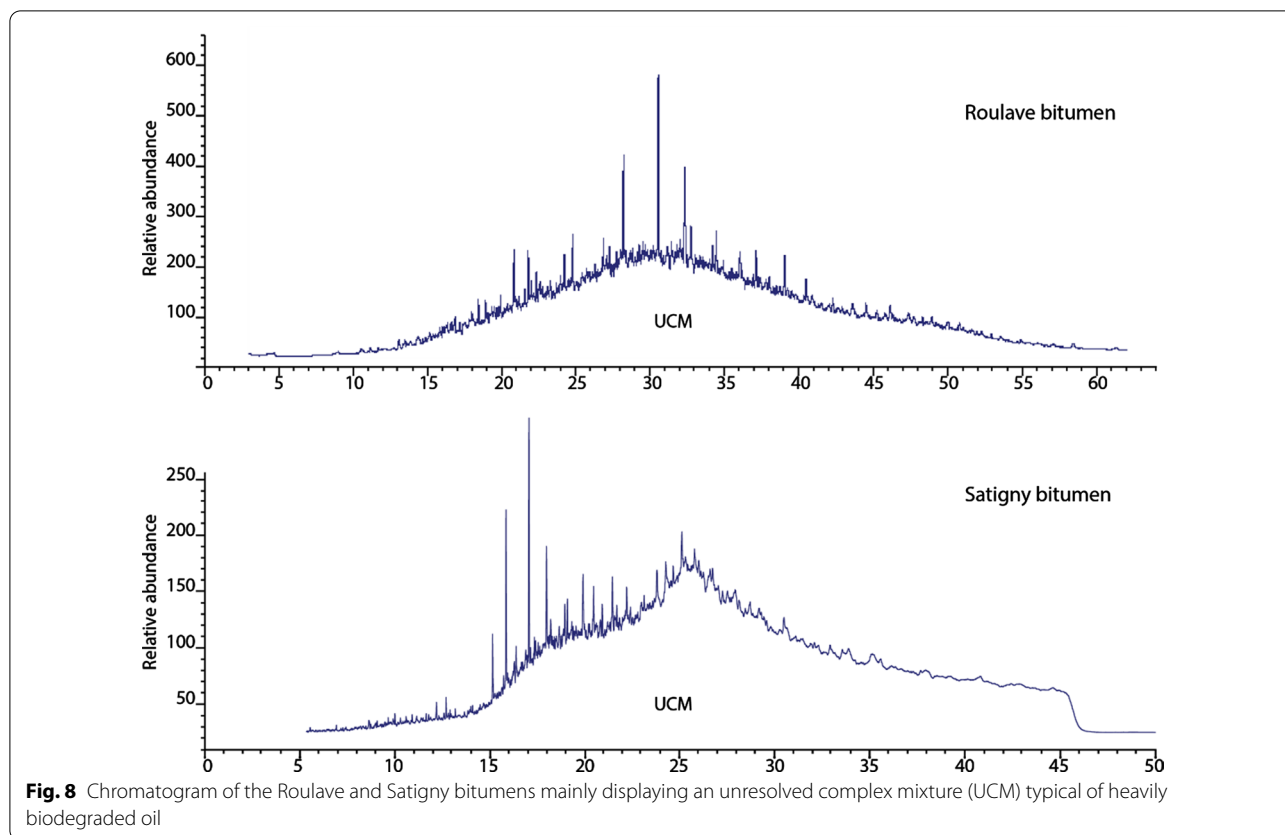


Table 5 Chemical and stable isotopic composition of the gas retrieved from Satigny

Components	Units	SAT1	SAT2	SAT1	SAT2	Hydrocarbons
		(100 µl)	(200 µl)	–	–	(average)–
CO	(Vol%)	0	0			
CO ₂	(Vol%)	0	0			
O ₂ + Ar	(Vol%)	3.16	4.09	–	–	–
Nitrogen	(Vol%)	11.55	14.86	–	–	–
				vol. % in 100 µL	vol. % in 200 µL	% C1–C6
Methane	(ppm)	2660	6114	53.2	61.14	98.87
Ethane	(ppm)	14.8	34.5	0.3	0.35	0.55
Propane	(ppm)	6.5	14.7	0.13	0.15	0.24
i-Butane	(ppm)	4.9	11.2	0.1	0.11	0.18
n-Butane	(ppm)	1.6	3.7	0.03	0.04	0.06
i-Pentane	(ppm)	1.1	2.6	0.02	0.03	0.04
n-Pentane	(ppm)	0	0.6	0	0.01	0.00
i-Hexane	(ppm)	1.5	1.6	0.03	0.02	0.04
n-Hexane	(ppm)	0.4	0.5	0.01	0.01	0.01
C1/(C2 + C3)		125	124			
δ ¹³ C-CH ₄	(‰ VPDB)	– 52.5	–			
δ ¹³ C-C ₂ H ₆	(‰ VPDB)	–	– 23.5			
δ ¹³ C-C ₃ H ₈	(‰ VPDB)	–	– 21.4			
δ ² H-CH ₄	(‰ SMOW)	–	– 231			

samples SAT1 and SAT2 as $C1/(C2 + C3)$ after Bernard et al. (1976). The mean dryness for both samples is 125.

The $\delta^{13}C$ value of methane ($\delta^{13}C\text{-CH}_4$) was measured in sample SAT1, while $\delta^{13}C$ of ethane and propane ($\delta^{13}C\text{-C}_2\text{H}_6$ and $\delta^{13}C\text{-C}_3\text{H}_8$) and δ^2H of methane ($\delta^2H\text{-CH}_4$) were measured in sample SAT2. $\delta^{13}C$ value of methane is at -52.5% vs. VPDB. $\delta^{13}C$ of ethane is at -23.5% vs. VPDB and $\delta^{13}C$ of propane is at -21.4% vs. VPDB. The Bernard diagram (Bernard et al. 1978) where the molecular ratio of $C1/(C2 + C3)$ is compared with the $\delta^{13}C\text{-CH}_4$ is widely used to distinguish between dry microbial and wet thermogenic gases. The Satigny gas composition does not fall within the pure microbial nor thermogenic gas fields and rather shows a mix between microbial and thermogenic gas (Fig. 9a). The stable isotopic carbon and hydrogen composition of methane reveals that the thermogenic gas is most likely originating from an early mature source-rock (Whiticar 1999) (Fig. 9b).

5 Discussion

5.1 Source rock maturity and kerogen type

5.1.1 Lias

In Switzerland as well as in W Germany, United Kingdom, Luxembourg or Netherlands, the Toarcian shales (Posidonia shales), equivalent to the Schistes Carton in SE France, consists of marine algal and bacterial Type II organic matter (Littke et al. 1988; Todorov et al. 1993; Röhl et al. 2001; Montero-Serrano et al. 2015; Song et al. 2015; Fantasia et al. 2019). In the northwestern and northeastern part of the Swiss Molasse Basin, the Toarcian shales are characterized by Type II organic matter, rather immature, yielding HI values up to 800 mgHC/gTOC (Fig. 5; Todorov et al. 1993; Fantasia et al. 2019). The thermal maturity of this source-rock primarily depends on its burial and one should expect greater maturity approaching the deepest part of the foreland basin toward the SE and the Alpine front thrusts (Leu and Gautschi 2014). This is clearly shown by the increase of maturity from the Geneva area to the subalpine molasse basin where vitrinite reflectance increases from 0.72 VRr% to <2.2 VRr% (Table 3). It is worth to note that the present-day burial depth of the source rock is lower than the maximum burial reached in the past considering the intense erosive event leading to a 2000–2600 m stratigraphic gap at the base of the Quaternary (Schegg et al. 1997; Moscariello et al. 2020b).

Looking at the HI vs. T_{\max} diagram (Fig. 5), it first appears that the Jurassic samples are in the oil window, except for the Chaleyriat-1 samples which are immature. This is confirmed by vitrinite reflectance measurements that indicate:

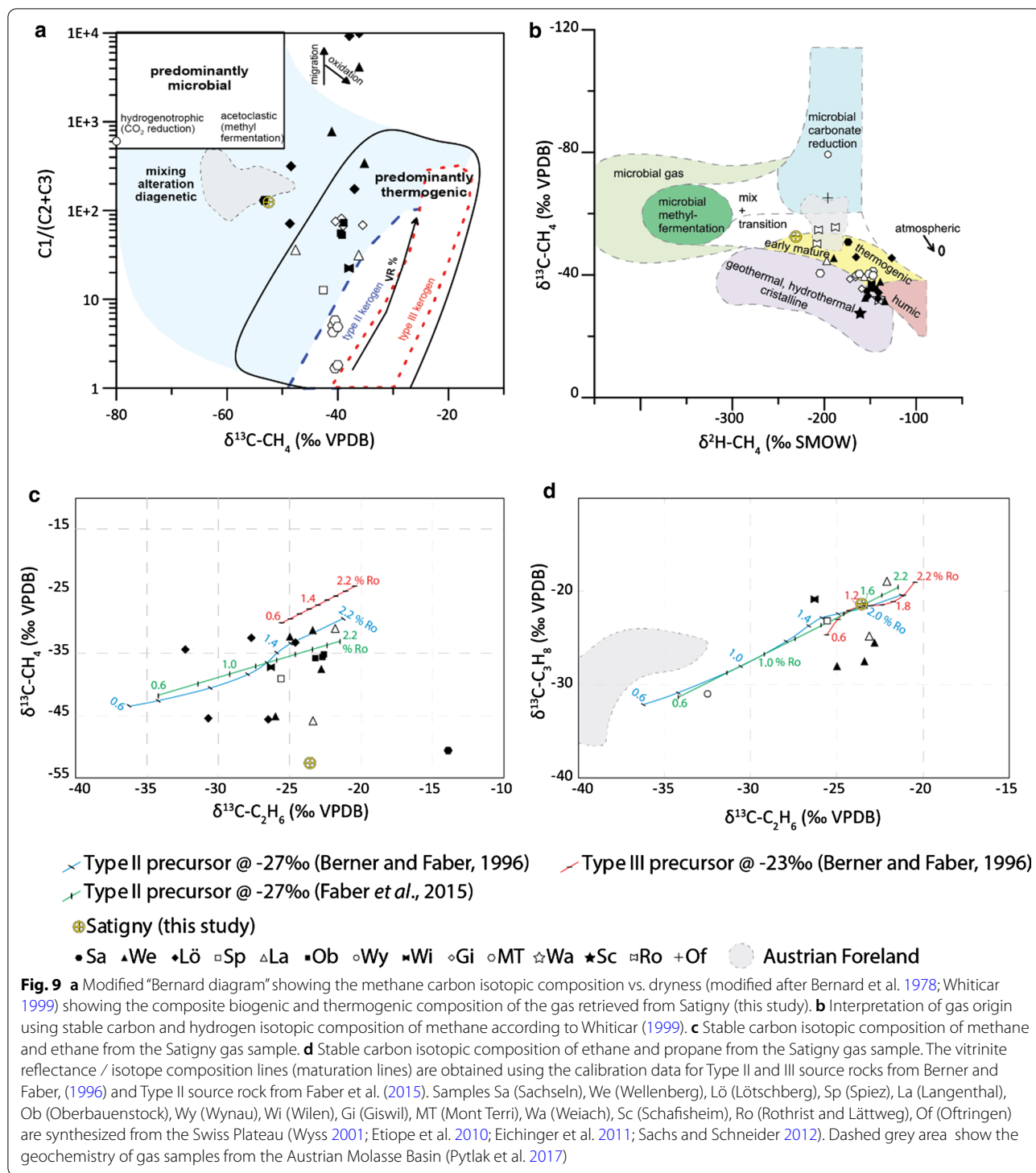
- All Lias samples from Humilly-2 and Chapeiry-1 wells reached oil window maturity ($Ro = 0.7\%$, T_{\max} around 440 °C),
- Samples from Faucigny-1 reached dry gas window maturity (equivalent $Ro > 2.2\%$, $T_{\max} > 515$ °C).

These statements are in agreement with a previous study (Deville and Sassi 2006) that also showed a strong difference in T_{\max} values between Lias from the Molasse plateau (≈ 440 °C) and from the Subalpine Molasse (> 500 °C).

No vitrinite reflectance measurements were made on the Chaleyriat-1 samples, but their much shallower depth (between 480 and 560 m) compared to other Liassic samples (minimum of 2100 m) are in agreement with their relatively low T_{\max} values (≤ 435 °C) indicating immaturity (Espitalié et al. 1985).

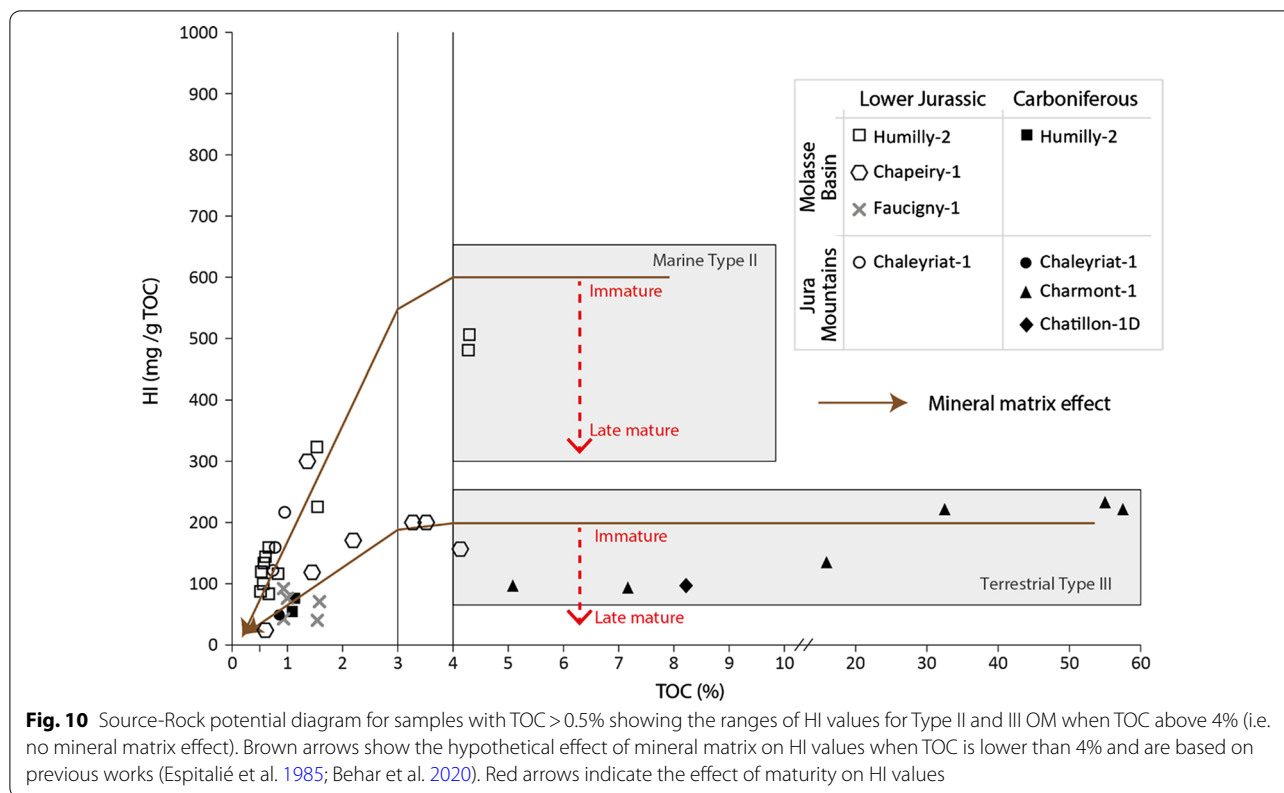
By examining the HI vs. T_{\max} diagram in more detail (Fig. 5), it also appears that 30 Liassic samples have a Type III OM, 6 samples from the Chapeiry-1 and Humilly wells have a mixture of Type II-III OM and 2 samples from the Humilly-2 well are of Type II. The two last samples from the Humilly-2 well (2238 and 2240) contain dominantly short-chain *n*-alkanes, typical for marine organic matter comparable to the immature Posidonia shales in the northwestern part of the Swiss Plateau (Elie and Mazurek 2008) (Fig. 6a, b). Moreover, biomarker ratios suggest that the 4 Liassic samples from the Humilly-2 well have the same origin (Fig. 7; Table 4). This also includes $Pr/n\text{-C}_{17}$ and $Ph/n\text{-C}_{18}$ ratio indicating a mixture of terrestrial and marine OM (Hunt 1996). Based on the above, it appears that there are contradictory interpretations for the 2 samples (2232 and 2236) with the lowest TOC and HI between biomarker and the HI vs. T_{\max} diagram. This may be due to the fact that, while the HI vs. T_{\max} diagram (Fig. 5) takes into account the effect of maturity on the HI values to assess the OM Type, it does not consider the MME that artificially lowers the S2 during pyrolysis for shale samples, and as a consequence, lowers the HI value of low TOC samples (Espitalié et al. 1984, 1985).

The HI vs. TOC diagram provides good insights on the MME (Fig. 10). Indeed, we can observe a clear correlation between HI and TOC, especially for Humilly-2 samples that are all mostly composed of shales. Then, using abacus proposed by previous studies including one for Toarcian samples from the Paris Basin (Espitalié et al. 1985; Behar et al. 2020), we can propose a hypothetical trend of MME on HI values with decreasing TOC (brown arrows in Fig. 10). For our study, these arrows clearly show that the Chaleyriat-1 and Humilly-2 samples are on the MME trend of the marine Type II, even though the last ones are in the early-oil window.



Chapeiry-1 samples are mostly made of shales, but two are carbonates: 3720.9 (HI=297 mg/g TOC) and 3722.7 (HI=198 mg/g TOC); their HI values are thus not affected by MME (Espitalié et al. 1985). These two samples are thus likely mixtures of Type II-III as

suggested by their biomarker profiles and ratios (i.e. relatively high TAR and mid-chain *n*-alkane concentrations), the terrestrial OM being more concentrated in sample 3722.7. All shale samples from the Chapeiry-1 well plot around the Type III MME trend, except one



(3728.8) that is under that trend. As their HI values are also affected by maturity, these samples are interpreted to be either mixtures of Type II-III or a degraded Type II like sample 3669. Biomarker distribution and ratios are similar to the Humilly-2 samples and typical of marine Type II OM. The Chapeiry-1 3728.8 sample shows dominance of aquatic biomarkers but with a relatively high contribution of terrestrial components. This sample is thus also probably a mixture of aquatic and terrestrial OM and its low HI (156 mg/g TOC) is likely due to a conjunction of maturity and MME, which, in some cases, can dramatically lower the HI values, even when TOC is above 4% (Saint-Germès et al. 2002). It is therefore clear that, during Liassic black shales deposition, the terrestrial inputs were stronger in the Chapeiry-1 area when compared to the Humilly-2 area. This may be due to the different location of the two wells compared to the basin margin: the Chapeiry-1 well penetrates a sequence which was originally closer to the paleo-shore or to turbidites nearby that can transport large amount of terrestrial OM (Biscara et al. 2011; Stetten et al. 2015).

Finally, the high thermal maturity of the Faucigny-1 samples makes it hard to decipher what was the original Type of OM.

5.1.2 Carboniferous

The maturity of the Molasse Basin Carboniferous formation can only be inferred from 3 of the Humilly-2 samples. Their T_{max} values range from 449 to 465 °C, suggesting a late oil to wet gas maturity, which is also supported by the VRr of 1.14% of sample 3039.8.

In the samples from the Jura wells, vitrinite reflectance values range between 0.6% and 0.8% suggesting that Carboniferous source-rocks are early to peak oil mature (Mukhopadhyay and Dow 1994; Mazurek et al. 2006). In the samples from the Charmont-1 well, we observe a clear increasing Ro trend with depth, from 0.6% at 1892 m to 0.79% at 2108 m, which indicates an evolution from early to peak oil. This is in agreement with the T_{max} values between 433 and 460 °C in this well (Espitalié et al. 1985). In the Chaleyriat area, Ro values all point to peak oil maturity, in agreement with the only reliable T_{max} value of 444 (Espitalié et al. 1985). The different maturities of Carboniferous source rocks between the Jura and the Geneva Basin are likely linked to their burial histories. Indeed, during the Oligocene-Pliocene, the Swiss Molasse Basin was marked by the deposition of large volumes of syntectonic flexural sediments that deeply buried Carboniferous to Eocene sediments (Deville and Sassi 2006) whereas the

Jura evolved at shallow levels forming the forebulge of the Alpine orogenic system (Sissingh 1998; Kuhlemann 2007).

Regarding the origin of the OM, biomarker distributions of the Geneva Basin samples show strong proportions of mid- and long-chain *n*-alkanes, indicating significant proportions of terrestrial OM (Peters et al. 2005). This is confirmed by TAR values of 0.93 and 2.5 (Bourbonniere and Meyers 1996). These values were probably even higher before catagenesis because with increasing maturity the *n*-alkanes distribution shifts towards lower-molecular-weight homologues (Peters et al. 2005). Regarding the Pr/*n*-C₁₇ vs. Ph/*n*-C₁₈ diagram (Fig. 7a), the Humilly-2 samples plot in the mixed OM domain (Hunt 1996), but increasing maturity tends to lower these ratios as more and more *n*-alkanes are produced during the catagenesis (Peters et al. 2005). In the HI vs. TOC diagram (Fig. 10), these samples also plot on the Type III trend, strengthening a terrestrial origin of the OM. In the HI vs. T_{max} diagram (Fig. 5) sample Humilly-2 3040.7 plots within the Type II-III domain, but such HI and T_{max} values are also reported for Carboniferous coals from the eastern Paris Basin (Espitalié et al., 1985) and the Ruhr Basin (Jasper et al. 2009).

The HI vs. TOC diagram (Fig. 10) indicates that all Carboniferous samples from the Jura region plot within the terrigenous Type III field. However, in the HI vs. T_{max} diagram (Fig. 5), some of the samples plot in the Type II-III and Type II domains. When looking at *n*-alkane distributions, sample Charmont-1 1894 is dominated by mid- and long-chain *n*-alkanes that display a clear odd over even predominance, which indicate that terrestrial plants are the main contributors of OM (Eglinton and Hamilton 1967). Compared to the Humilly-2 samples, the sample Charmont-1 1894 shows higher mid-chain and lower long-chain concentrations. This indicate that macrophytes were mainly aquatic or emerged in the Charmont-1 well location, whereas they were land plant in the Jura region as well as in Humilly-2 (Ficken et al. 2000). Moreover, Pr/*n*-C₁₇ vs. Ph/*n*-C₁₈ values (Fig. 7a) also indicate a terrestrial OM dominance for this Charmont-1 sample (Hunt 1996). In other Chamont-1 samples, HC distributions are similar to the Humilly-2 Toarcian samples suggesting that there are marine or lacustrine OM inputs (Peters et al. 2005). This is also suggested by the HI and T_{max} values (Fig. 5). Similar contradictory ratios are also observed for the Chatillon-1D sample with Rock-Eval data indicating a Type III OM, whereas HC distributions and biomarker ratios indicate significant marine inputs. While enhanced maturity may have influenced biomarker ratios for other samples, Chatillon-1D samples are less mature than Humilly-2 ones and biomarker ratios should provide valid information (Fang et al. 2019).

To our knowledge, despite a recent attempt of identifying Carboniferous to Permian paleoenvironments in the Jura (Pullan and Berry 2019) at present there are no reliable studies that would help to decipher the origin of the OM during that geological time interval. In western Europe, the latter is punctuated by the collapse of the Variscan mountain range, causing the development of a complex landscape characterized by the formation of several hemi-graben and graben basins filled with terrestrial and lacustrine sediments such as in the French Central Massif and the Saar Nahe Basin where major coal seams and oil shales accumulated (Ziegler 1990; Müller et al. 2006; Schneider et al. 2006; Izart et al. 2012). Furthermore, a recent study of the Autun basin, located 120 km in the northeast from the Jura, revealed that Gzhelian and Asselian oil shales are associated with lacustrine and/or terrestrial degraded OM (Garel et al. 2017). Carboniferous-Permian deposits found in the Jura area might then be comparable to the ones observed in the lacustrine Autun basin where the oil-shales and coal seams shows similar TOC and maturities to the ones observed in our study (Garel et al. 2017). Thus, the contradictory data observed here might reflect the influence of terrestrial and lacustrine OM during sediment deposition, such as in the Autun basin. Yet, the low HI values of our samples indicate that the terrestrial OM is dominant in these potential compositional mixtures. To prove that, additional analyzes such as further biomarker studies or palynofacies observations should be carried out.

5.2 Implications for the regional petroleum system

5.2.1 Source-rock potentials

The majority of analyzed Liassic samples has TOC values below 2% and genetic potential (i.e. S1 + S2) values below 1.1 mg HC/g rock, indicating very poor to poor petroleum generation potential (Peters and Cassa 1994;

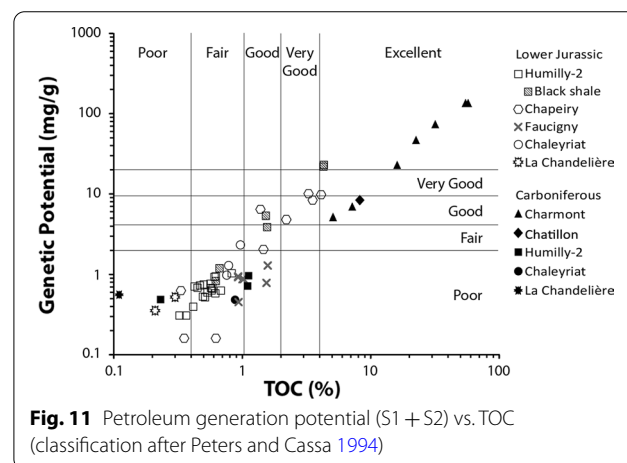


Fig. 11). However, this set of samples includes the 7 Chapeiry-1 samples (representing 15% of the total Liassic samples) that are highly mature and have thus probably already generated and expelled hydrocarbons (Espitalié et al., 1985).

Samples with a higher potential are all from the Humilly-2 (4 samples) and Chapeiry-1 wells (7 samples). Overall, the source-rock potential has been found fair for 3 samples, good for 4 samples, very good from 2 samples from the Chapeiry-1 well and excellent for 2 samples from the Humilly-2 well (Peters and Cassa 1994; Fig. 11).

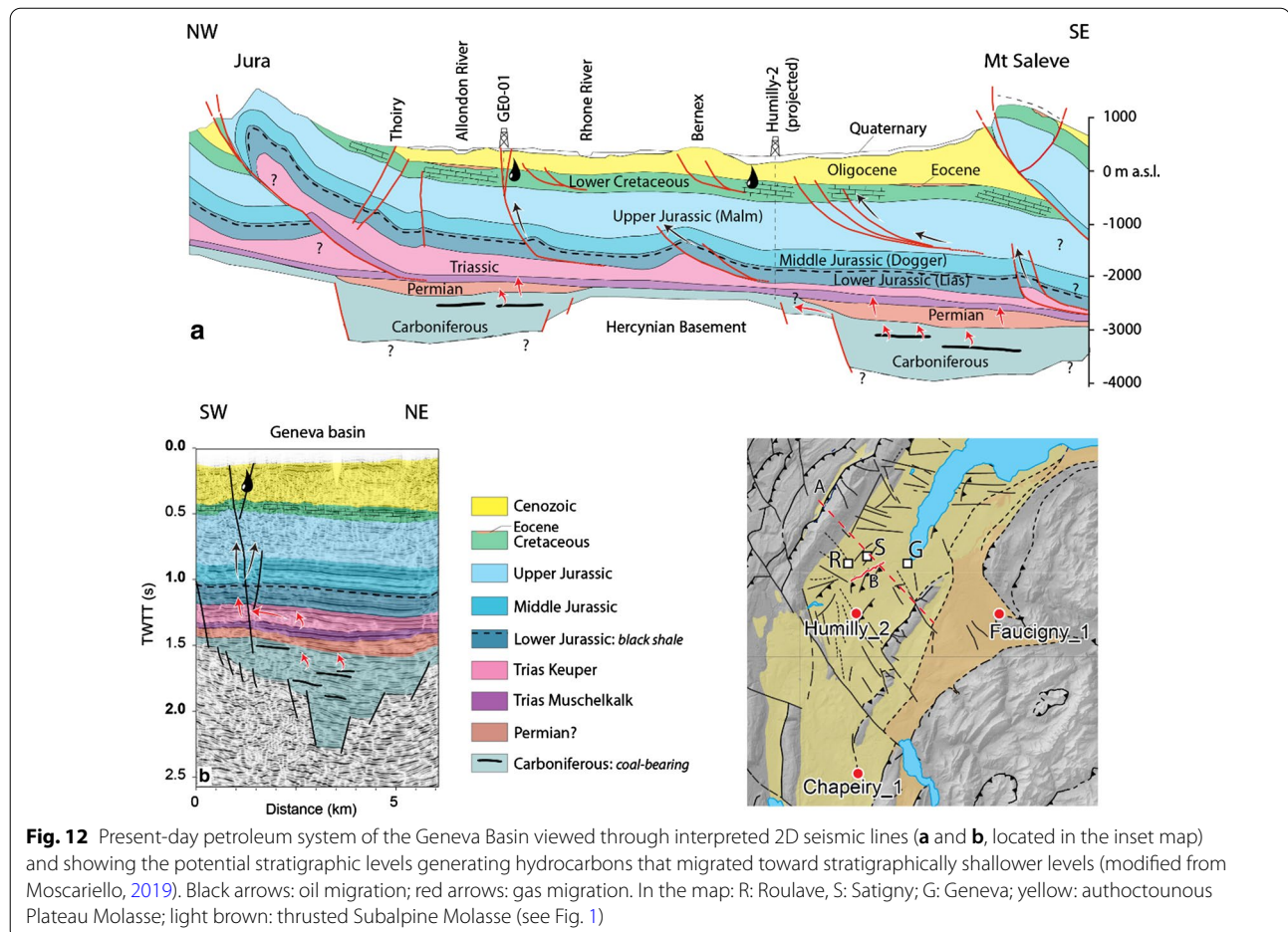
In summary, the above data indicate that while Lower Jurassic source-rocks are immature in the Jura region, they are in the oil or gas window in the Molasse Basin. In this basin, most rocks show no or only poor potential, but 26% of the studied rocks display at least a fair potential for oil (marine OM) and gas (mixed marine and terrestrial OM) generation and 15% have likely produced and expelled gas (highly mature Type III).

The Carboniferous source rock potential is poor for Humilly-2 samples (Fig. 11), but their maturities suggest that they already generated and expelled hydrocarbons

accounting for a significant part of their initial potential (Espitalié et al. 1985); therefore, their original potential was (much) higher. Charmont-1 and Chatillon-1D coal samples display good to excellent source rock potential for gas, as they are mostly dominated by terrestrial OM (Fig. 11). Thus, while all Carboniferous Molasse Basin samples have a poor potential, 80% of Jura samples have at least a good potential for gas. It should be noted that only the superficial part of the Carboniferous grabens have been reached with the wells (only 3 m in Humilly-2) and that most of it remains buried (Fig. 12a). Coal seams are most likely deposited occurring in the deep grabens and may therefore be mature enough (i.e. > 1.3 VRR%) to generate dry gas.

5.2.2 Oil and gas characterization and origin

The unresolved complex mixture of the bitumen chromatograms from the Roulave and Satigny does not allow a detailed geochemical interpretation on the origin of these former crude oils. Nevertheless, the resolved regular steranes (C_{27} to C_{29}) for the Roulave bitumen plot in the regular steranes ternary diagram within the open marine



depositional environment, and very close to the Toarcian shales sterane relative abundance (Fig. 7b). Unfortunately, no peaks were resolved for the Satigny bitumen. Most of the oil and impregnations from the Vaud canton (North of the study area) are originating from the Toarcian shales, except for the Eclépens quarry where a more mature source rock is expected (Dolivo 2016). Interestingly, Pullan and Berry (2019) interpreted the oil found in the La Chandelière-1 well as originating from a very mature lacustrine Permian shale (VRr ~ 1%) assumed to be present at depth. Given the present-day maturity trend of the overburden source rock and the burial history (Schegg et al. 1999) we can infer that the Roulave bitumen derives from the Toarcian source rock but we can't discard the contribution of a Permian lacustrine source rock present at depth, as suggested by seismostratigraphic data (Moscariello 2019).

The stable carbon isotopic composition of methane (Fig. 9a) and the gas dryness ($C_1/(C_2 + C_3)$) of gas from Satigny indicate a mix of thermogenic and microbial origin. However, geochemistry of bitumen from Satigny indicates biodegradation, which may have influenced the gas composition as well because secondary microbial gas associated with degradation of petroleum or bitumen can show similar gas composition (Milkov 2011, 2018; Milkov and Etiope 2018). This gas composition is close to the one of the Lötschberg tunnel (black diamond in Fig. 9a) or from the Austrian Foreland Basin (Pytlak et al. 2017) all being characterized by a mixture of thermogenic and microbial gas. The stable carbon and hydrogen isotopic compositions of methane from Satigny (Fig. 9b) are comparable to the gas samples retrieved in Rothrist located at the northern border of the Swiss Plateau (Sachs and Schneider 2012), where deep Permo-Carboniferous troughs are supposed to be the source-rock of the thermogenic gas component. Interestingly, such mixture of gas has also been evidenced in the Austrian North Alpine Foreland Basin: Misch et al. (2017) showed that the gas retrieved from shallow depth is mainly composed of microbial gas (primary and partly altered) mixed with deep thermogenic gas (originating from Triassic and Permian sequences).

Plots of $\delta^{13}C$ of methane versus $\delta^{13}C$ of ethane, and $\delta^{13}C$ of ethane versus $\delta^{13}C$ of propane (Berner and Faber 1996; Fig. 9c, d) are often used to determine the organic precursor and thermal maturity of the gas. Due to contribution of microbial methane, the isotopic composition of methane is not helpful to determine any organic precursor for the thermogenic component of the Satigny gas (Fig. 9c). Similar results have been obtained in the Swiss Plateau (in Sachseln and Lötschberg; Wyss, 2001) and interpreted as the result of microbial influence. Etiope et al. (2010) interpreted the lack of significant

concentrations of C_{3+} alkanes in the Giswil gas seep as the result of biodegradation. Clear evidence of biodegradation has been found in the bitumen sample encountered at Satigny with the gas (Fig. 8). Biodegradation may have affected the Satigny gas as well, but a more detailed study including $\delta^{13}C$ -CO₂ measurement would be required to support this interpretation.

The stable carbon isotopic composition of ethane and propane from Satigny does not show any microbial contribution or biodegradation related shifts as in the Austrian Foreland Basin (Pytlak et al. 2017). Maturity trends of Type II and III precursors show that the Satigny gas can originate either from an overmature Type II (from ~ 1.6 to 2.0 VRr%) or a mature Type III source rock (~ 1.2VRr%, Fig. 9d). It is important to note that no information exists about the isotopic data of potential precursor kerogen in the study area; therefore, we used the isotope ratios for sapropelic and humic kerogens used by Berner and Faber (1996) as guideline. In the Geneva Basin, the two major source-rocks identified in this study, namely the dominantly Type II Toarcian and the dominantly Type III Carboniferous, are in the early-oil window and early-gas window, respectively. There is no indication of overmature marine Type II source rocks at depth. Thus, the gas retrieved at Satigny likely originates from Carboniferous source rock bearing Type III kerogen. To reinforce this assumption, the high iC_4/nC_4 ratio of the sample from Satigny supports an origin from early mature type III kerogen (Connan and Cassou 1980).

The terrigenous origin of the Satigny gas is also in agreement with gas found in wells drilled in the Jura region and gas seeps at Cuarny and at Essertines for which a Type III thermogenic source with a maturity < 1.5% VRr (Pullan and Berry 2019). A comparable origin has been put forward for the origin of gas from the Weiach and Schafisheim wells (Hinze et al. 1986) located above deep Permo-Carboniferous grabens in the northeastern Swiss Plateau. The Giswil and Wilen gas seeps identified by Wyss (2001) and Etiope et al. (2010) in the southern limb of the Swiss Plateau seem to be in turn originating from a Type II thermogenic source with a maturity < 1.5% VRr. This shows the complexity of the petroleum systems acting below the Swiss Plateau.

5.2.3 Implications for geothermal exploration

The occurrence of mature marine and terrigenous OM in the Geneva Basin subsurface is of importance for the geothermal exploration as (1) the reservoir targets of the Upper Jurassic and Lower Cretaceous carbonates can be impregnated or partly filled by hydrocarbons as it has been shown in the Lower Cretaceous (Moscariello 2019) and (2) unexpected gas pockets can be encountered at variable depths during the drilling

operations, thus representing a potential risk with negative impact on safety and overall exploration costs.

Given the geometry of the Geneva Basin, a foreland setting with the foredeep located to the SE close to the northwestern margin of the Alpine front, hydrocarbons mostly migrate up-dip from the SE to NW. This explains why most of the oils seeps are located at the northwestern tip of the Molasse Basin (Leu 2012; Moscariello et al. 2020b). However, the Geneva Basin is highly faulted and cross-cut by several NW–SE left-lateral strike-slip faults and NE–SW thrust faults accommodating the recent compressional deformation of the Alpine arc (Moscariello 2019). This structural pattern may both (1) facilitate the formation of structural traps in the basin and (2) prevent from large accumulations of hydrocarbons at depth in case of leaking. Most of the thrust faults are rooted in intermediate marly stratigraphic units within the Lower Cretaceous and Middle Jurassic (Moscariello 2019), the deepest ones being rooted in the evaporites of the Keuper (Fig. 12) that supposedly act as a regional seal (Fig. 2). Those faults may act as preferential pathways for the hydrocarbons generated at depth (Fig. 12), specifically in the case of the marine Type II-derived oil. Although the organic-rich Toarcian shales in the Geneva Basin have a fair to excellent petroleum potential (Fig. 11), their limited thickness not exceeding 8 m in the Humilly-2 well, combined with the likely absence of large and structural traps, make the encountering of large hydrocarbon accumulations a low risk for the deep geothermal exploration.

Seismic reflection profiles below the Geneva Basin show the occurrence deep grabens most likely filled by Permo-Carboniferous rocks (Fig. 12a, b; Moscariello 2019). There, both the lacustrine Permian shales and the coal-bearing Carboniferous shales would be in the gas window at present-day and surely represent the stratigraphic interval of highest chance of conventional gas accumulations below the Triassic seal, as it has been revealed further east in the St Gallen area (Omodeo-Salé et al. 2020). However, as indicated before, the seal integrity at this level could have been severely affected and weakened by the large amount of faults developed during the Alpine shortening which cross the entire stratigraphic succession. This can explain why deep Type III-derived gas have reached the topmost stratigraphic levels in the Molasse. It has been documented that the Permo-Carboniferous itself may act as tight gas reservoirs as in Noville (Leu 2012) as well as the Buntsandstein (Moscariello 2019). In this respect, a 3D basin modeling study will be required to model and quantify the circulation, saturation and potential stratigraphic/structural traps in the entire Geneva Basin.

6 Conclusions

Two major source-rocks have been identified in the Geneva Basin, the dominantly marine Type II Toarcian (Lower Jurassic) shales and the terrigenous Type III Carboniferous.

The Toarcian source-rock is immature in the Jura region, in the oil window in the Geneva Basin and over-mature at the front of the Alpine thrust. Rock–Eval pyrolysis combined with gas chromatography indicate that this source-rock is composed of a mixture of Type II and III organic matter, the latter being more influent towards the Jura and the South of the basin (Chapeiry-1). The petroleum potential of the Toarcian shales is fair to excellent, but its limited thickness and the dense network of faults and fractures in the area did not favor accumulation and preservation of petroleum generated by this source-rock and hence the risk for the geothermal exploration is low.

The Carboniferous source-rock is at least in the oil window in the Jura and in the late oil-wet gas window in the Geneva Basin. Pyrolysis and geochemical indicators reveal that this source-rock mostly contains Type III organic matter with slight to significant marine or lacustrine OM inputs. Even though the present-day potential below the Geneva Basin is rather low because it already expelled hydrocarbons, it may have charged large accumulations that would represent high risk for geothermal exploration. As highlighted by our study, gas pocket can be encountered at shallow depth, demonstrating the ability of hydrocarbons generated at depth to migrate through the entire stratigraphic succession.

The bitumen sampled in the Roulave stream seems to be derived from the marine Type II Toarcian shales as indicated by the relative abundance of regular steranes (C_{27} to C_{29}). On the other hand, the origin of bitumen retrieved from Satigny shallow borehole cannot be identified, due to the high degree of biodegradation. It might either originate from the marine Type II Toarcian shales or from the Permian lacustrine shales as shown previously in the Jura region. Given the maturity of the identified marine and terrigenous source-rocks, the gas sampled in the Satigny borehole most likely derives from a mature terrigenous Type III organic matter such as the Carboniferous source-rock.

Acknowledgements

This paper is a contribution to the UNCONGAS project supported by swisstopo, the Swiss Federal Office of Energy, the Canton of Geneva and the Canton of Vaud and the SCCER SoE national research program funded by the SNF and Innosuisse. The authors would like to thank Gunter Siddiqi (SFOE) and Roland Baumberger (swisstopo) who initiated and encouraged this project. NAGRA (Nationale Genossenschaft für die Lagerung radioaktiver Abfälle) is also thanked for sharing its technical reports, SEAG and Werner Leu for sharing their data and knowledge.

We are thankful to Alexei Milkov, Werner Leu and the editor Wilfried Winkler for their constructive review that helped improve the manuscript.

Table 6 List of the sampled intervals in the various wells of the study area

Humilly-2			Humilly-2			Humilly-2			Humilly-2			Humilly-2			Humilly-2		
Depth	Age	Type	Depth	Age	Type	Depth	Age	Type	Depth	Age	Type	Depth	Age	Type	Depth	Age	Type
70	Oligocène	Cut	682	Valang.	Cut	1015.5	Kimmeridgian	Plug	1857.3	Bathonian	Plug	2250	Pliensbachian	Cut	2900	Muschelkalk	Cut
103		Cut	702		Cut	1020.5		Plug	1860.8		Plug	2252		Cut	2904.7		Frag
140		Cut	722	Cut	1024	Cut		1864	Cut		2270	Cut		2905.5	Frag		
170		Cut	750	Cut	1052	Cut		1900	Cut		2290	Cut		2907	Plug		
190		Cut	774	Cut	1108	Cut		1912	Cut		2310	Cut		2907.4	Plug		
230		Cut	Berriasian	Cut	1122	Cut		1932	Cut		2330	Cut		2908	Plug		
260		Cut		782	Cut	1144		Cut	1952		Cut	2342		Cut	2910		Plug
280		Cut		Cut	1176	Cut		1976	Cut		2360	Cut		2916.6	Plug		
310		Cut		790	Cut	1206		Cut	1997.3		Plug	2400		Cut	2917.2		Frag
340		Cut		800	Cut	1230		Cut	2000.1		Frag	2440		Cut	2922.5		Plug
360		Cut		808	Cut	1300		Cut	2001.2		Plug	2469.3		Plug	2925.1		Frag
380		Cut		812	Cut	1350		Cut	2003.5		Plug	2480		Cut	2927.8		Plug
410		Cut		816	Cut	1402		Cut	2012		Cut	2500		Cut	2929.1		Frag
430		Eocène		Cut	824	Tithonian		Cut	1450		Cut	2520		Cut	2930.3		Plug
432	Cut			832	Cut		1504	Cut	2088	Plug	2529.1	Cut	2942				
458	Barremian	Cut		840	Cut		1550	Cut	2104	Plug	2529.3	Plug	2951.4	Plug			
		Cut		848	Cut		1574	Cut	2116	Cut	2532	Frag	2958.5	Plug			
Cut		856		Cut	1604		Cut	2128	Cut	2536	Cut	2966.1	Plug				
Cut		868		Cut	1652		Cut	2146	Cut	2540	Cut	2966.2	Plug				
490		Cut	876	Cut	1700		Cut	2156	Cut	2543	Cut	2980	Cut				
513		Cut	884	Cut	1742		Cut	2174	Cut	2546	Cut	2990	Cut				
538		Cut	892	Cut	1808		Cut	2182	Cut	2549	Cut	3020	Cut				
550		Cut	904	Cut	1846		Cut	2190	Cut	2580	Cut	3027	Cut				
		Cut	940	Cut	1852.4		Plug	2200	Cut	2610	Cut	3028.3	Plug				
		Cut	958	Cut	1853.2		Frag	2212	Cut	2640	Cut	3034.5	Frag				
562		Hauterivian	Cut	994	Cut		1854.6	Plug	2228	Cut	2670	Cut	3035	Plug			
582			Cut	978	Cut		2230	Cut	2710	Cut	3037.4	Plug					
602			Cut	2232	Cut	2726	Cut	3037.5	Frag								
622			Cut	2234	Cut	2742	Cut	3038	Plug								
642	Cut		2236	Cut	2752	Cut	3038.5	Plug									
658	Cut		2238	Cut	2782	Cut	3039.3	Frag									
			2240	Cut	2812	Cut	3040.7	Frag									
					2842	Cut	3049	Cut									
					2862	Cut											
					2884	Cut											

cuttings, core fragments, core plug

Author's contributions

DDC conducted the whole study, performed the sampling, the seismic interpretation and the Rock-Eval pyrolysis; SG bring his expertise on multi-proxies organic geochemistry interpretations; AM supervised the project and brings his expertise in the Geneva Basin geology; SBD and RL performed the vitrinite reflectance and GC-MS analysis; PW performed the gas geochemistry analysis. All authors discussed the results and contributed to the final manuscript. All authors read and approved the final manuscript.

Competing interests

The authors declare that they have no competing interests.

Author details

¹ Sorbonne Université, CNRS-INSU, Institut Des Sciences de La Terre Paris, IStEP UMR 7193, 75005 Paris, France. ² CVA Engineering, Immeuble Toki Lana, 7, chemin de la Marouette, Bayonne, France. ³ Energy and Geoscience Institute, University of Utah, 423 Wakara Way, Salt Lake City, USA. ⁴ Department of Earth Science, University of Geneva, Rue des Maraichers, 13 - 1205 Geneva, Switzerland. ⁵ Institute of Geology and Geochemistry of Petroleum and Coal, EMR Group, RWTH Aachen University, 52056 Aachen, Germany. ⁶ Federal Institute for Geosciences and Natural Resources (BGR), Stillweg 2, Hannover, Germany. ⁷ Present Address: Beicip-Franlab, 232 avenue Napoleon Bonaparte, 92500 Rueil-Malmaison, France.

Appendix 1

See Table 6.

References

Baudin, F., Herbin, J.-P., & Vandenbroucke, M. (1990). Mapping and geochemical characterization of the Toarcian organic matter in the Mediterranean Tethys and Middle East. *Organic Geochemistry*, 16(4), 677–687. [https://doi.org/10.1016/0146-6380\(90\)90109-D](https://doi.org/10.1016/0146-6380(90)90109-D).

Behar, F., Beaumont, V., & Pentead, De. B. (2001). Rock-Eval 6 technology: performances and developments. *Oil & Gas Science and Technology*, 56(2), 111–134. <https://doi.org/10.2516/ogst:2001013>.

Behar, F., Delhaye-Prat, V. & Garel, S. (2020). Detritic input quantification in lacustrine petroleum systems: example of the pre-salt source rocks from the Lower Congo Basin. The Depositional Record.

Bernard, B. B., Brooks, J. M., & Sackett, W. M. (1976). Natural gas seepage in the Gulf of Mexico. *Earth and Planetary Science Letters*, 31(1), 48–54.

Bernard, B. B., Brooks, J. M., & Sackett, W. M. (1978). Light hydrocarbons in recent Texas continental shelf and slope sediments. *Journal of Geophysical Research: Oceans*, 83(C8), 4053–4061. <https://doi.org/10.1029/JC083iC08p04053>.

Berner, U., & Faber, E. (1996). Empirical carbon isotope/maturity relationships for gases from algal kerogens and terrigenous organic matter, based on dry, open-system pyrolysis. *Organic Geochemistry*, 24(10), 947–955. [https://doi.org/10.1016/S0146-6380\(96\)00090-3](https://doi.org/10.1016/S0146-6380(96)00090-3).

Biscara, L., Mulder, T., Martinez, P., Baudin, F., Etcheber, H., Jouanneau, J.-M., & Garlan, T. (2011). Transport of terrestrial organic matter in the Ogooué deep sea turbidite system (Gabon). *Marine and Petroleum Geology*, 28(5), 1061–1072. <https://doi.org/10.1016/j.marpetgeo.2010.12.002>.

Bou Daher, S., Nader, F. H., Müller, C., & Littke, R. (2015). Geochemical and petrographic characterization of Campanian-Lower Maastrichtian calcareous petroleum source rocks of Hasbayya, South Lebanon. *Marine and Petroleum Geology*, 64, 304–323. <https://doi.org/10.1016/j.marpetgeo.2015.03.009>.

Bourbonniere, R. A., & Meyers, P. A. (1996). Sedimentary geolipid records of historical changes in the watersheds and productivities of Lakes

- Ontario and Erie. *Limnology and Oceanography*, 41(2), 352–359. <https://doi.org/10.4319/lo.1996.41.2.0352>.
- Bray, E. E., & Evans, E. D. (1961). Distribution of n-paraffins as a clue to recognition of source beds. *Geochimica et Cosmochimica Acta*, 22(1), 2–15. [https://doi.org/10.1016/0016-7037\(61\)90069-2](https://doi.org/10.1016/0016-7037(61)90069-2).
- Bruns, B., Littke, R., Gasparik, M., van Wees, J.-D., & Nelskamp, S. (2016). Thermal evolution and shale gas potential estimation of the Wealden and Posidonia Shale in NW-Germany and the Netherlands: a 3D basin modelling study. *Basin Research*, 28(1), 2–33. <https://doi.org/10.1111/bre.12096>.
- Burri, P. (2010). A revolution in gas: the rise of the unconventional. *Swiss Bulletin für angewandte Geologie*, 15(2), 35–44.
- Burri, P., Chew, K., Jung, R., & Neumann, V. (2011). The Potential of Unconventional Gas—energy bridge to the future. *Swiss Bulletin für angewandte Geologie*, 16(2), 3–55.
- Capar, L., Couëffé, R., Brenot, A., Courrioux, G., Dezayes, C., Gabalda, S., Lopez, S., Marc, S., Rambourg, D., Siméon, Y., Andenmatten, N., Clerc, N., Meyer, M., & Rusillon, E. (2015). GeoMol - Évaluation des ressources naturelles dans les bassins d'avant-chaîne alpins pour une utilisation et une gestion durable du sous-sol - Zone Pilote Genève-Savoie. (BRGM, Ed. Vol. BRGM 64744-FR). BRGM. <http://infoterre.brgm.fr/rapports/RP-64744-FR.pdf>.
- Charollais, J., Weidmann, M., Berger, J. P., Engesser, B., Hotellier, J. F., Reichenbacher, B., & Schäfer, P. (2007). La Molasse du bassin franco-genevois et son substratum. *Archives des Sciences Genève*, 60, 59–174.
- Chelle-Michou, C., Do Couto, D., Moscarriello, A., Renard, P., & Rusillon, E. (2017). Geothermal state of the deep Western Alpine Molasse Basin, France-Switzerland. *Geothermics*, 67, 48–65. <https://doi.org/10.1016/j.geothermics.2017.01.004>.
- Chevalier, G., Diamond, L. W., & Leu, W. (2010). Potential for deep geological sequestration of CO₂ in Switzerland: a first appraisal. *Swiss Journal of Geosciences*, 103(3), 427–455. <https://doi.org/10.1007/s00015-010-0030-4>.
- Chew, K. (2010). *The shale frenzy comes to Europe* (p. 8). New York: E&P Magazine.
- Connan, J., & Cassou, A. M. (1980). Properties of gases and petroleum liquids derived from terrestrial kerogen at various maturation levels. *Geochimica et Cosmochimica Acta*, 44(1), 1–23. [https://doi.org/10.1016/0016-7037\(80\)90173-8](https://doi.org/10.1016/0016-7037(80)90173-8).
- Deville, E., & Sassi, W. (2006). Contrasting thermal evolution of thrust systems: An analytical and modeling approach in the front of the western Alps. *AAPG Bulletin*, 90(6), 887–907. <https://doi.org/10.1306/01090605046>.
- Dolivo, E. (2016). Prospectivity of the Gros-de-Vaud permit (Canton of Vaud - Switzerland). Ascent Resources plc. Unpublished report for the Direction générale de l'environnement (DGE), Canton of Vaud, Lausanne.
- Eglinton, G., & Hamilton, R. J. (1967). Leaf Epicuticular Waxes. *Science*, 156(3780), 1322–1335. <https://doi.org/10.1126/science.156.3780.1322>.
- Eichinger, F., Eichinger, L., & Ertl, S. (2011). Genese der leichten Kohlenwasserstoffe im Opalinuston des Felslabors Mont Terri. (NAGRA, Ed. Vol. NAB 11–33).
- Elie, M., & Mazurek, M. (2008). Biomarker transformations as constraints for the depositional environment and for maximum temperatures during burial of Opalinus Clay and Posidonia Shale in northern Switzerland. *Applied Geochemistry*, 23(12), 3337–3354. <https://doi.org/10.1016/j.apgeochem.2008.05.022>.
- Espitalié, J., Deroo, G., & Marquis, F. (1985). La pyrolyse Rock-Eval et ses applications. *Première partie. Rev. Inst. Fr. Pét.*, 40(5), 563–579. <https://doi.org/10.2516/ogst:1985035>.
- Espitalié, J., Laporte, J. L., Madec, M., Marquis, F., Leplat, P., Paulet, J., & Boutefeu, A. (1977). Méthode rapide de caractérisation des roches mères, de leur potentiel pétrolier et de leur degré d'évolution. *Rev. Inst. Fr. Pét.*, 32(1), 23–42. <https://doi.org/10.2516/ogst:1977002>.
- Espitalié, J., Senga Makadi, K., & Trichet, J. (1984). Role of the mineral matrix during kerogen pyrolysis. *Organic Geochemistry*, 6, 365–382. [https://doi.org/10.1016/0146-6380\(84\)90059-7](https://doi.org/10.1016/0146-6380(84)90059-7).
- Etiopie, G., Zwahlen, C., Anselmetti, F. S., Kipfer, R., & Schubert, C. J. (2010). Origin and flux of a gas seep in the Northern Alps (Giswil, Switzerland). *Geofluids*, 10(4), 476–485. <https://doi.org/10.1111/j.1468-8123.2010.00302.x>.
- Faber, E., Schmidt, M., & Feyzullayev, A. (2015). Geochemical hydrocarbon exploration—insights from stable isotope models. *Oil & Gas Journal*, 41(2), 93–98. <http://oceanrep.geomar.de/28994/>
- Fang, R., Littke, R., Zieger, L., Baniasad, A., Li, M., & Schwarzbauer, J. (2019). Changes of composition and content of tricyclic terpane, hopane, sterane, and aromatic biomarkers throughout the oil window: A detailed study on maturity parameters of Lower Toarcian Posidonia Shale of the Hils Syncline NW Germany. *Organic Geochemistry*, 138, 103928. <https://doi.org/10.1016/j.orggeochem.2019.103928>.
- Fantasia, A., Föllmi, K. B., Adatte, T., Spangenberg, J. E., & Mattioli, E. (2019). Expression of the Toarcian Oceanic Anoxic Event: New insights from a Swiss transect. *Sedimentology*, 66(1), 262–284. <https://doi.org/10.1111/sed.12527>.
- Ficken, K. J., Li, B., Swain, D. L., & Eglinton, G. (2000). An n-alkane proxy for the sedimentary input of submerged/floating freshwater aquatic macrophytes. *Organic Geochemistry*, 31(7), 745–749. [https://doi.org/10.1016/S0146-6380\(00\)00081-4](https://doi.org/10.1016/S0146-6380(00)00081-4).
- Garel, S., Behar, F., Schnyder, J., & Baudin, F. (2017). Palaeoenvironmental control on primary fluids characteristics of lacustrine source rocks in the Autun Permian Basin (France). *Bulletin de la Société Géologique de France*, 188, 5. <https://doi.org/10.1051/bsgf/2017187>.
- Gorin, G. E., Signer, C., & Amberger, G. (1993). Structural configuration of the Western Swiss Molasse Basin as defined by reflection seismic data. *Eclogae Geologicae Helveticae*, 86(3), 693–716.
- Grohmann, S., Romero-Sarmiento, M.-F., Nader, F. H., Baudin, F., & Littke, R. (2019). Geochemical and petrographic investigation of Triassic and Late Miocene organic-rich intervals from onshore Cyprus, Eastern Mediterranean. *International Journal of Coal Geology*, 209, 94–116. <https://doi.org/10.1016/j.coal.2019.05.001>.
- Hinze, W., Jaeggi, K., & Schenker, F. (1986). Exploratory boreholes Boettstein, Weiach, Riniken, Schafisheim, Kaisten, Leuggern: gas measurements. (NAGRA, Ed. Vol. NTB 86–11).
- Hunt, J. M. (1996). *Petroleum geochemistry and geology*. W.H. Freeman.
- IEA (2015). World Energy Outlook 2015. OECD Publishing. <https://doi.org/10.1787/weo-2015-en>
- Izart, A., Palhol, F., Gleixner, G., Elie, M., Blaise, T., Suarez-Ruiz, I., et al. (2012). Palaeoclimate reconstruction from biomarker geochemistry and stable isotopes of n-alkanes from Carboniferous and Early Permian humic coals and limnic sediments in western and eastern Europe. *Organic Geochemistry*, 43, 125–149. <https://doi.org/10.1016/j.orggeochem.2011.10.004>.
- Izart, A., Barbarand, J., Michels, R., & Privalov, V. A. (2016). Modelling of the thermal history of the Carboniferous Lorraine Coal Basin: Consequences for coal bed methane. *International Journal of Coal Geology*, 168, 253–274. <https://doi.org/10.1016/j.coal.2016.11.008>.
- Jasper, K., Krooss, B. M., Flajs, G., Hartkopf-Fröder, C., & Littke, R. (2009). Characteristics of type III kerogen in coal-bearing strata from the Pennsylvanian (Upper Carboniferous) in the Ruhr Basin, Western Germany: Comparison of coals, dispersed organic matter, kerogen concentrates and coal-mineral mixtures. *International Journal of Coal Geology*, 80(1), 1–19. <https://doi.org/10.1016/j.coal.2009.07.003>.
- Jenkyns, H. C. (1988). The early Toarcian (Jurassic) anoxic event; stratigraphic, sedimentary and geochemical evidence. *American Journal of Science*, 288(2), 101–151. <https://doi.org/10.2475/ajs.288.2.101>.
- Kuhlemann, J. (2007). Paleogeographic and paleotopographic evolution of the Swiss and Eastern Alps since the Oligocene. *Global and Planetary Change*, 58(1), 224–236. <https://doi.org/10.1016/j.gloplacha.2007.03.007>.
- Lagotala, H. (1932). Les gîtes bitumineux de Dardagny (Genève). *Le Globe. Revue genevoise de géographie*, 3–109. https://www.persee.fr/doc/globe_0398-3412_1932_num_71_1_2646
- Landis, C. R., & Castaño, J. R. (1995). Maturation and bulk chemical properties of a suite of solid hydrocarbons. *Organic Geochemistry*, 22(1), 137–149. [https://doi.org/10.1016/0146-6380\(95\)90013-6](https://doi.org/10.1016/0146-6380(95)90013-6).
- Lahusen, P. H. (1992). Hydrocarbon exploration in the Swiss Molasse Basin. *Eclogae Geologicae Helveticae*, 85(3), 707–714.
- Leu, W. (2008). Potential der Kohlenwasserstoffressourcen Schweizer Mittelland und subalpinen Bereich (NAGRA, Ed. Vol. NAB 08–35, pp. 15).
- Leu, W. (2012). Swiss oil/gas exploration and lessons learnt. *Swiss Bulletin für angewandte Geologie*, 17(1), 49–59.
- Leu, W., & Gautschi, A. (2014). The Shale Gas Potential of the Opalinus Clay and Posidonia Shale in Switzerland – A First Assessment. *Swiss Bull. angew. Geol.*, 19(2), 95–107.
- Leu, W., & Siddiqi, G. (2013). CO₂ sequestration in Switzerland? *Swiss Bulletin für angewandte Geologie*, 18(2), 105–113.
- Littke, R., Baker, D. R., & Leythaeuser, D. (1988). Microscopic and sedimentologic evidence for the generation and migration of hydrocarbons in Toarcian source rocks of different maturities. In L. Mattavelli & L. Novelli (Eds.),

- Organic Geochemistry In Petroleum Exploration (pp. 549–559). <https://doi.org/10.1016/B978-0-08-037236-5.50061-0>
- Littke, R., Krooss, B., Uffmann, A. K., Schulz, H.-M., & Horsfield, B. (2011). Unconventional gas resources in the paleozoic of Central Europe. *Oil Gas Sci Technol*, 66(6), 953–977. <https://doi.org/10.2516/ogst/2010033>.
- Madritsch, H., Naef, H., Meier, B., Franzke, H. J., & Schreurs, G. (2018). Architecture and Kinematics of the Constance-Frick Trough (Northern Switzerland): Implications for the Formation of Post-Variscan Basins in the Foreland of the Alps and Scenarios of Their Neogene Reactivation. *Tectonics*, 37(7), 2197–2220. <https://doi.org/10.1029/2017tc004945>.
- Matte, P. (2001). The Variscan collage and orogeny (480–290 Ma) and the tectonic definition of the Armorica microplate: a review. *Terra Nova*, 13(2), 122–128. <https://doi.org/10.1046/j.1365-3121.2001.00327.x>.
- Mazurek, M., Hurford, A. J., & Leu, W. (2006). Unravelling the multi-stage burial history of the Swiss Molasse Basin: integration of apatite fission track, vitrinite reflectance and biomarker isomerisation analysis. *Basin Research*, 18(1), 27–50. <https://doi.org/10.1111/j.1365-2117.2006.00286.x>.
- McCann, T., Pascal, C., Timmerman, M. J., Krzywiac, P., López-Gómez, J., Wetzell, L., et al. (2006). Post-Variscan (end Carboniferous–Early Permian) basin evolution in Western and Central Europe. *Geological Society, London, Memoirs*, 32(1), 355–388. <https://doi.org/10.1144/gsl.mem.2006.032.01.22>.
- Milkov, A. V. (2011). Worldwide distribution and significance of secondary microbial methane formed during petroleum biodegradation in conventional reservoirs. *Organic Geochemistry*, 42(2), 184–207. <https://doi.org/10.1016/j.orggeochem.2010.12.003>.
- Milkov, A. (2018). Secondary microbial gas. Hydrocarbons, oils and lipids: Diversity, origin, chemistry and fate: Handbook of hydrocarbon and lipid microbiology: Springer, Cham, Switzerland, 1–10.
- Milkov, A. V., & Etiope, G. (2018). Revised genetic diagrams for natural gases based on a global dataset of >20,000 samples. *Organic Geochemistry*, 125, 109–120. <https://doi.org/10.1016/j.orggeochem.2018.09.002>.
- Misch, D., Leu, W., Sachsenhofer, R. F., Gratzner, R., Rupprecht, B., & Bechtel, A. (2017). Shallow hydrocarbon indications along the Alpine thrust belt and adjacent foreland basin : distribution and implications for petroleum exploration. *Journal of Petroleum Geology*, 40(4), 341–362. <https://doi.org/10.1111/jpg.12684>.
- Montero-Serrano, J.-C., Föllmi, K. B., Adatte, T., Spangenberg, J. E., Tribouillard, N., Fantasia, A., & Suan, G. (2015). Continental weathering and redox conditions during the early Toarcian Oceanic Anoxic Event in the north-western Tethys: Insight from the Posidonia Shale section in the Swiss Jura. *Palaeogeography, Palaeoclimatology, Palaeoecology*, 429, 83–99. <https://doi.org/10.1016/j.palaeo.2015.03.043>.
- Moscariello, A. (2019). Exploring for geo-energy resources in the Geneva Basin (Western Switzerland): opportunities and challenges. *Swiss Bulletin für angewandte Geologie*, 24(2), 105–124. <https://archive-ouverte.unige.ch/unige:131617>
- Moscariello, A., Guglielmetti, L., Omodeo Sale, S., De Haller, A., Eruteya, O., Lo, H. Y., Clerc, N., Makhlofi, Y., Do Couto, D., Ferreira De Oliveira, G., Perozzi, L., De Oliveira Filho, F., Hollmuller, P., Quiquerez, L., Nawratil De Bono, C. F., Martin, F., & Meyer, M. (2020a). Heat production and storage in Western Switzerland: advances and challenges of intense multidisciplinary geothermal exploration activities, an 8 years progress report. In Proceedings World Geothermal Congress (pp. 12). <https://archive-ouverte.unige.ch/unige:127903>
- Moscariello, A., Do Couto, D., Omodeo Salé, S. (2020b). An analysis of the petroleum system in the Swiss Molasse Basin with a focus on Western Switzerland (UNCONGAS). Rep Swiss geol. Surv. 100 in press.
- Mukhopadhyay, P. K., & Dow, W. G. (1994). Vitrinite reflectance as a maturity parameter: applications and limitations. *American Chemical Society Series* 570.
- Müller, A. B., Strauss, H., Hartkopf-Fröder, C., & Littke, R. (2006). Reconstructing the evolution of the latest Pennsylvanian–earliest Permian Lake Odernheim based on stable isotope geochemistry and palynofacies: A case study from the Saar-Nahe Basin, Germany. *Palaeogeography, Palaeoclimatology, Palaeoecology*, 240(1), 204–224. <https://doi.org/10.1016/j.palaeo.2006.03.049>.
- Omodeo-Salé, S., Eruteya, O. E., Cassola, T., Baniasad, A., & Moscariello, A. (2020). A basin thermal modelling approach to mitigate geothermal energy exploration risks: The St. Gallen case study (eastern Switzerland). *Geothermics*, 87:101876. <https://doi.org/10.1016/j.geothermics.2020.101876>
- Peters, K. E., & Cassa, M. R. (1994). Applied Source-Rock Geochemistry. In L. B. Magoon & W. G. Dow (Eds.), *The Petroleum System. From Source to Trap* (pp. 93–120). American Association of Petroleum Geologists.
- Peters, K. E., Walters, C. C., & Moldowan, J. M. (2005). *The Biomarker Guide. Volume 1: Biomarkers and Isotopes in the Environment and Human History. Volume 2: Biomarkers and Isotopes in Petroleum Exploration and Earth History. Second Edition.* Cambridge University Press.
- Pullan, C. P., & Berry, M. (2019). A Paleozoic-sourced oil play in the Jura of France and Switzerland. *Geological Society, London, Special Publications*, 471(1), 365–387. <https://doi.org/10.1144/sp471.2>.
- Pytlak, L., Gross, D., Sachsenhofer, R. F., Bechtel, A., & Linzer, H. G. (2017). Gas accumulations in Oligocene-Miocene reservoirs in the Alpine Foreland Basin (Austria): evidence for gas mixing and gas degradation. *International Journal of Earth Sciences*, 106(6), 2171–2188. <https://doi.org/10.1007/s00531-016-1421-1>.
- Röhl, H.-J., Schmid-Röhl, A., Oschmann, W., Frimmel, A., & Schwark, L. (2001). The Posidonia Shale (Lower Toarcian) of SW-Germany: an oxygen-depleted ecosystem controlled by sea level and palaeoclimate. *Palaeogeography, Palaeoclimatology, Palaeoecology*, 165(1), 27–52. [https://doi.org/10.1016/S0031-0182\(00\)00152-8](https://doi.org/10.1016/S0031-0182(00)00152-8)
- Sachs, O., & Schneider, N. (2012). Auftreten von Kohlenwasserstoffen in der Region des Jura-Südfusses (Abschnitt Aarwangen – Baden). (NAGRA, Ed. Vol. NAB 12–32).
- Saint-Germès, M., Baudin, F., Bazhenova, O., Derenne, S., Fadeeva, N., & Largeau, C. (2002). Origin and preservation processes of amorphous organic matter in the Maykop Series (Oligocene–Lower Miocene) of Precaucasus and Azerbaijan. *Bulletin de la Société Géologique de France*, 173(5), 423–436. <https://doi.org/10.2113/173.5.423>.
- Schegg, R., Cornford, C., & Leu, W. (1999). Migration and accumulation of hydrocarbons in the Swiss Molasse Basin: implications of a 2D basin modeling study. *Marine and Petroleum Geology*, 16(6), 511–531. [https://doi.org/10.1016/S0264-8172\(99\)00018-5](https://doi.org/10.1016/S0264-8172(99)00018-5).
- Schegg, R., Leu, W., Cornford, C., & Allen, P. A. (1997). New coalification profiles in the Molasse Basin of Western Switzerland: Implications for the thermal and geodynamic evolution of the Alpine Foreland. *Eclogae Geologicae Helveticae*, 90(1), 79–96.
- Schneider, J. W., Körner, F., Roscher, M., & Kroner, U. (2006). Permian climate development in the northern peri-Tethys area — The Lodève basin, French Massif Central, compared in a European and global context. *Palaeogeography, Palaeoclimatology, Palaeoecology*, 240(1), 161–183. <https://doi.org/10.1016/j.palaeo.2006.03.057>.
- Schoenherr, J., Littke, R., Urai, J. L., Kukla, P. A., & Rawahi, Z. (2007). Polyphase thermal evolution in the Infra-Cambrian Ara Group (South Oman Salt Basin) as deduced by maturity of solid reservoir bitumen. *Organic Geochemistry*, 38(8), 1293–1318. <https://doi.org/10.1016/j.orggeochem.2007.03.010>.
- Shanmugam, G. (1985). Significance of Coniferous Rain Forests and Related Organic Matter in Generating Commercial Quantities of Oil, Gippsland Basin, Australia. *AAPG Bulletin*, 69(8), 1241–1254. <https://doi.org/10.1306/ad462bc3-16f7-11d7-8645000102c1865d>.
- Sherwood, O. A., Schwietzke, S., Arling, V. A., & Etiope, G. (2017). Global inventory of gas geochemistry data from fossil fuel, microbial and burning sources, version 2017. *Earth System Science Data*, 9, 639–656.
- Signer, C., & Gorin, G. E. (1995). New geological observations between the Jura and the Alps in the Geneva area, as derived from reflection seismic data. *Eclogae Geologicae Helveticae*, 88(2), 235–265.
- Sissingh, W. (1998). Comparative Tertiary stratigraphy of the Rhine Graben, Bresse Graben and Molasse Basin: correlation of Alpine foreland events. *Tectonophysics*, 300(1), 249–284. [https://doi.org/10.1016/S0040-1951\(98\)00243-1](https://doi.org/10.1016/S0040-1951(98)00243-1).
- Sommaruga, A., Eichenberger, U., & Marillier, F. (2012). *Seismic Atlas of the Swiss Molasse Basin.* (S. G. Commission, Ed. Vol. Matér. Géol. Suisse, Géophys. 44.). Swiss Geophysical Commission.
- Sommaruga, A., Mosar, J., Schori, M., & Gruber, M. (2017). Chapter 20 - The Role of the Triassic Evaporites Underneath the North Alpine Foreland. In J. I. Soto, J. F. Flinch, & G. Tari (Eds.), *Permo-Triassic Salt Provinces of Europe, North Africa and the Atlantic Margins* (pp. 447–466). Elsevier. <https://doi.org/10.1016/B978-0-12-809417-4.00021-5>
- Song, J., Littke, R., Weniger, P., Ostertag-Hennin, C., & Nelskamp, S. (2015). Shale oil potential and thermal maturity of the Lower Toarcian Posidonia

- Shale in NW Europe. *International Journal of Coal Geology*, 150–151, 127–153. <https://doi.org/10.1016/j.coal.2015.08.011>.
- Stetten, E., Baudin, F., Reyss, J.-L., Martinez, P., Charlier, K., Schnyder, J., et al. (2015). Organic matter characterization and distribution in sediments of the terminal lobes of the Congo deep-sea fan: Evidence for the direct influence of the Congo River. *Marine Geology*, 369, 182–195. <https://doi.org/10.1016/j.margeo.2015.08.020>.
- Todorov, I., Schegg, R., & Wildi, W. (1993). Thermal maturity and modelling of Mesozoic and Cenozoic sediments in the south of the Rhine Graben and the eastern Jura (Switzerland). *Eclogae Geologicae Helveticae*, 86, 667–692.
- Taylor, G. H., Teichmüller, M., Davis, A., Diessel, C. F. K., Littke, R., & Robert, P. (1998). *Organic Petrology* (p. 704). Stuttgart Germany: Schweizerbart Science Publishers.
- Weniger, P., Blumenberg, M., Berglar, K., Ehrhardt, A., Klitzke, P., Krüger, M., & Lutz, R. (2019). Origin of near-surface hydrocarbon gases bound in northern Barents Sea sediments. *Marine and Petroleum Geology*, 102, 455–476. <https://doi.org/10.1016/j.marpetgeo.2018.12.036>.
- Whiticar, M. J. (1999). Carbon and hydrogen isotope systematics of bacterial formation and oxidation of methane. *Chemical Geology*, 161(1), 291–314. [https://doi.org/10.1016/S0009-2541\(99\)00092-3](https://doi.org/10.1016/S0009-2541(99)00092-3).
- Wyss, R. (2001). Der Gasausbruch aus einer Erdsondenbohrung in Wilen (OW). *Bulletin für Angewandte Geologie*, 6, 25–40.
- Ziegler, P. A. (1990). Geological atlas of western and central Europe. (G. S. London, Ed. 2nd ed.). Shell Internationale Petroleum Maatschappij B.V.

Publisher's Note

Springer Nature remains neutral with regard to jurisdictional claims in published maps and institutional affiliations.

Submit your manuscript to a SpringerOpen[®] journal and benefit from:

- Convenient online submission
- Rigorous peer review
- Open access: articles freely available online
- High visibility within the field
- Retaining the copyright to your article

Submit your next manuscript at ► [springeropen.com](https://www.springeropen.com)
